Geological constraints on Archean (3.22 Ga) coastal-zone processes from the Dycedale Syncline, Barberton Greenstone Belt

C. Heubeck
Friedrich-Schiller-Universität Jena, Burgweg 11, 07749 Jena, Germany;
e-mail: christoph.heubeck@uni-jena.de

S. Bläsing and M. Grund
Institut für Geologische Wissenschaften, Freie Universität Berlin, 12249 Berlin, Germany;
e-mail: s.blaesing@live.de; m.grund@live.de

N. Drabon
Department of Geosciences, Stanford University, CA 94305-2115, USA;
e-mail: drabon@stanford.edu

M. Homann
Institut für Geologische Wissenschaften, Freie Universität Berlin, 12249 Berlin, Germany;
now at: Institut Universitaire Européen de la Mer, 29280 Plouzané, France;
e-mail: martin.homann@univ-brest.fr

S. Nabhan
Institut für Geologische Wissenschaften, Freie Universität Berlin, 12249 Berlin, Germany;
now at: Institut für Geowissenschaften, Universität Jena, 07749 Jena, Germany
e-mail: sami.nabhan@fu-berlin.de

Abstract

Geological constraints bearing on Paleoarchean surface environments are rare but critical, establishing the physiological consequences of a very different physical environment for early life, including a different tectonic style, closer Earth-Moon interaction, different chemical composition of atmosphere and hydrosphere, higher weathering intensity, and to validate geochemical proxy data. Strata relevant to these topics can be studied in uniquely accessible, subvertically dipping beds of the Moodies Group (ca. 3.22 Ga) within the tightly folded, steeply plunging western Dycedale Syncline of the Barberton Greenstone Belt. They display a large variety of environment-specific sedimentary structures in a small (ca. 1 km^2) but excellently exposed area, including microbial mats, abundant shoreline and tidal structures and early diagenetic pedogenic nodules. These are set among conglomerates, sandstones, minor lava flows and banded-iron formation within an initially deepening-, then shallowing-upward sequence, including (from base to top) braided-fluvial floodplain, sandy shoreline, and estuarine and protected tidal environments, some of which were temporally choked by volcanic ash. Shorelines were (semi-)arid, had fluctuating groundwater levels and moderate to high tides. Nevertheless, diverse microbial communities gained footholds in this challenging setting, including sulfate reducers in the shallow subsurface, photosynthesizers along high-energy shorelines, and photoferrotrophs or other Fe-metabolizing chemolithautotrophs in lagoonal or offshore settings.

Facies analysis and regional structural geology suggest that the Dycedale area formed a minor, structurally controlled basin within a southward-facing fold-and-thrust belt which became intensely deformed during subsequent steepening. Overall, the datasets derived from this area allow the detailed description of interactions between early Earth's volcanism, atmo- and hydrosphere and place the emergent biosphere into physical settings that are observable to such detail in only few other places worldwide.

Introduction

Reconstructions of Earth's Archean surface conditions not only expand our knowledge of the origin and development of early life on Earth and of the interaction between Earth's atmo-, hydro- and geosphere with an emergent biosphere, but also allow us to understand non-actualistic conditions which may have existed on other planets. Thus, Archean greenstone belts, deformed remnants of volcano-sedimentary strata set among voluminous adjacent magmatic rocks, are prime objectives for paleoenvironmental studies in deep time. Strata of the Barberton Greenstone Belt of the Kapvaal craton, Mpumalanga, South Africa, are among the foremost geoscientific archives (e.g., Lowe and Byerly, 2007). While numerous studies have focused on the volcanology and geochemistry of mafic and ultramafic rocks from the Onverwacht Group at the base of the greenstone belt's stratigraphic column and the convergent-margin-style units of the overlying Fig Tree Group (e.g., Lowe and Nocita, 1999), comparatively few studies have interpreted the strata of the topmost Moodies Group in terms of Archean surface conditions.

This manuscript extends our knowledge of Paleoarchean surface processes by describing and interpreting geological field data from a small but excellently exposed and accessible segment of Moodies strata in the Dycedale Syncline of the Barberton Greenstone Belt.

Regional geology

The Moodies Group of the Barberton Greenstone Belt (BGB; ~3.57 to ~3.22 Ga; Figure 1), South Africa and Swaziland, is the oldest well-preserved siliciclastic shallow-water unit on Earth and is well-known for its strata deposited in alluvial, fluvial, shoreline, tidal and deltaic settings (Hall, 1918; Visser et al., 1956; Anhaeusser, 1976; Eriksson, 1977, 1978, 1979, 1980; Heubeck and Lowe, 1994a, b, 1999; Hessler and Lowe, 2006; Heubeck, 2009). It forms the uppermost part of the Barberton Supergroup (the greenstone belt's volcano-sedimentary fill) and is exposed in large, northeast-southwest-trending synclines up to 15 km long and several km wide. These are tightly folded and plunge moderately to steeply. Moodies strata resist weathering compared to adjacent strata of the underlying Fig Tree and Onverwacht Groups and to plutonic rocks adjacent to the greenstone belt, and consequently form steep-sided rocky hills and nearly all of the highest mountains of the Barberton Mountain Land. Because of the tight folding of all BGB strata, most outcrops show beds on-end.

The Moodies Group reaches up to 3.5 km thick and consists dominantly of quartz-rich sandstones. Siltstones make up approximately half of the stratigraphic column in some parts of the BGB but generally crop out poorly. Conglomerates and shales are subordinate; BIF, jaspilite, and volcanics constitute a minor lithologic component. Strata are dominated by thick alluvial, fluvial, deltaic, tidal and arguably eolian deposits. Deep-water, below-wavebase deposits, mostly in prodelta-facies, are common in some regions, while alluvial environments appear to be largely restricted to the base and the top of the stratigraphic column. Jaspilites, shales and siltstones represent deposition below wavebase but the preponderance of current- and wave-reworked structures suggest that most deposition occurred close to or above sea level. Zircon ages from thin volcanic tuffs at the base and the top of the Moodies Group overlap each other within analytical error and suggest that the Moodies Group was likely deposited within only ~1 to 10 Myr between approx. 3224 and 3214 Ma (Heubeck et al., 2013). The end of deposition, along with deformation, may have occurred as early as 3220 Ma. The low degree of observed facies variability implies a stable balance between high subsidence and high sedimentation rates, with a mean depositional rate of m/ka. If cryptic disconformities and hiatuses, generally not uncommon in terrestrial and marginal marine environments, are factored in, depositional rates may even have been substantially higher. The available data thus suggest that Moodies strata record a very-high-resolution record of Archean terrestrial, coastal, and shallow-shelf processes.

Dycedale Syncline: Location, structure, alteration

Location

Dycedale Syncline is a comparatively small, narrow and elongate, tightly folded and steeply southwestward-plunging syncline in Fig Tree and Moodies strata in the central BGB, located on Farms Wonderscheur 362 JU and Dycedale 368 JU east of Barberton (Figures 1, 2). It is wedged between the much larger Saddleback Syncline to the south and the Ulundi Syncline to the north and separated from these by the Barbrook Fault to the north and the Saddleback Fault to the south, respectively. These two major faults merge just south of Barberton. Both faults progressively truncate the limbs of the Dycedale Syncline in a westwardly narrowing apex. The Barbrook Fault also truncates the fold axis of the Dycedale Syncline.

Most of the area underlain by strata of the Dycedale Syncline is occupied by the broad, east-west-trending valley of Hislop's Creek where strata are poorly exposed. Thus, the eastern termination and the central segment of the syncline on Farms Wonderscheur 362 JU and parts of Dycedale 368 JU, respectively, are poorly known (Figure 2; Lowe et al., 2012). Its westernmost end, however, north of Saddleback Hill (1640 m), is excellently exposed on steep, north- and northeast-facing slopes on Farm Dycedale 368 JU. The area, shown in Figures 2 to 4, includes the steeply southwest-plunging synclinal axis, flanked by upward-facing northern and overturned southeastern limbs, which each expose strata of ca. 500 m thickness.

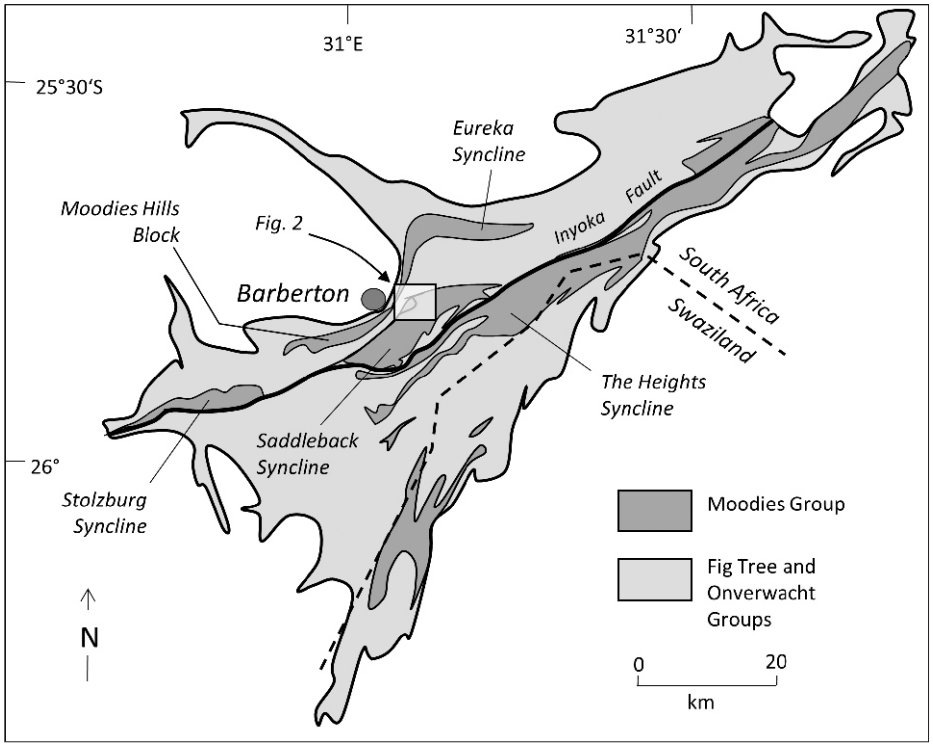

Figure 1. *Location of study area within the Barberton Greenstone Belt (BGB). Rectangle shows area of Figure 2.*

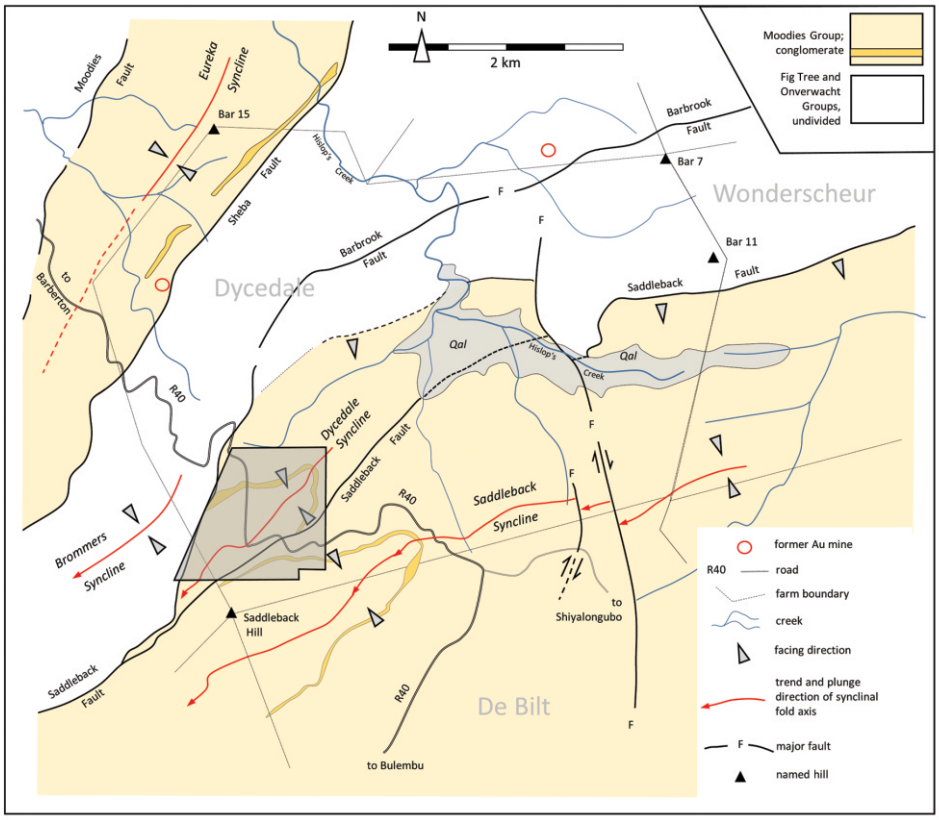

Figure 2. *Geologic map showing tectonic position of the Dycedale Syncline. The Saddleback Fault separates the Dycedale Syncline from the much larger Saddleback Syncline to the south, the Barbrook Fault from the Brommers and Ulundi (not shown) Synclines to the north. Hislop's Creek drains poorly exposed strata of the central and eastern parts of the syncline. The western part of the syncline, subject of this study (shaded rectangle shows detailed geologic map; Figure 3), is wedged between the southwestward-converging Saddleback and Barbrook Faults, plunges steeply southwest and is excellently exposed on the steep slopes north of Saddleback Hill.*

This small area of slightly more than 1 km^2 in size, the subject of this manuscript, has been a classical stop of geological field trips traversing the BGB (e.g., Pearton, 1986; Ashwal, 1991; Lowe and Byerly, 2003; Ferrar and Heubeck, 2013; Heubeck et al., 2016), typically with the objective to present examples of sedimentary processes in Archean shallow-water settings. Eriksson (1978, 1979, 1980) drew upon outcrop examples from this region and Eriksson et al. (2006) described and interpreted a partial stratigraphic measured section across a prominent ridge ("Geologist's Ridge") on the southeastern limb of the syncline. Noffke et al. (2006) based descriptions of Archean microbial mats largely on evidence from the same ridge, and Homann (2016) inferred terrestrial settings for an occurrence of microbial mats in a prominent conglomerate. However, the western Dycedale Syncline area was not mapped in detail (1:1,500 scale; Bläsing et al., 2015; Grund, 2015) until recently.

Structure and strain

The study area represents the southwestward-narrowing apex of a triangle defined by the converging Barbrook and Saddleback Faults. The northern, east-west trending limb of Dycedale Syncline dips moderately to steeply south; the southeastern limb is overturned and dips steeply southeast (Figure 3). The synclinal fold axis plunges about 50 to 65° towards the southwest; measurements near the hinge indicate that the axis may be segmented.

Grains and minerals in hand samples and thin sections of sandstone and volcanics show only a weak alignment defining foliation, typical of many other Moodies strata (Gay, 1969; Anhaeusser, 1969; Lamb, 1987; Heubeck and Lowe, 1994a). Measurements of conglomerate clast shape on the limbs of Dycedale Syncline (Gay, 1969; Heubeck and Lowe, 1994b; Bläsing, 2015) suggest that ductile strain is very low. However, detailed geological mapping (Bläsing et al., 2015) indicates that the stratigraphic thickness, in particular of fine-grained, incompetent, recessively weathering, poorly exposed units nearly doubles in the hinge zone, which may be due to small-scale internal faulting there, recrystallization at grain scale, and bedding-parallel flexural-slip. However, some Moodies strata are clearly syndeformational (Lamb, 1987; Heubeck and Lowe, 1994b), suggesting that some thickness variations may in part be primary.

Metamorphism and alteration

Even though there are no specific data on metamorphic grade from the Dycedale Syncline, the region is likely to have experienced similar conditions as the remainder of the greenstone belt (De Ronde and De Wit, 1994; Ward, 1995; Toulkeridis et al., 1998; Tice et al., 2004). The BGB has undergone regional lower-greenschist-facies metamorphism with peak metamorphic conditions to 350 ± 50°C; muscovite and chlorite are widespread in the metamorphic mineral assemblage. Chloritoid occurs as a metamorphic mineral in shaly sandstones south of the Inyoka Fault but has not been documented north of this fault. The presence of chloritoid is rather non-specific and indicates temperatures between 220°C in Fe-rich pelites, which is the chloritoid-in reaction in Fe-rich metapelites (the temperature is somewhat higher in "normal" metapelites), and 550°C, which represents the chloritoid-out reaction (Bucher and Frey, 1994). Raman spectroscopy on kerogenous material from the Moodies Group of the adjacent Saddleback Syncline suggests maximum temperatures of 330 to 470°C, consistent with data from vitrinite reflectance (>300°C) and rock-eval pyrolysis (332 to 338°C) (Heubeck et al., 2015). XRF analysis of kaolinite-rich sandstones from the Dycedale Syncline yield unambiguous kaolinite peaks. Overall, maximum metamorphic temperatures were likely above 280°C but did not exceed 450°C.

Moodies strata have undergone several phases of post-depositional alteration including carbonization, sericitization and silicification (Heubeck and Lowe, 1999; Nabhan et al., 2016a). Owing to the widespread early silicification of many strata, compaction was low and sedimentary structures are generally excellently preserved.

Methods

We geologically mapped the westernmost Dycedale Syncline at a scale of 1:1,500 and measured detailed stratigraphic columns on both limbs of the syncline. Paleocurrents from foresets were corrected for synclinal plunge and dip of bedding using Stereonet 9.2.0 (Allmendinger et al., 2013). Natural ionizing radiation was measured using a hand-held Geiger-Muller tube (Radiation Alert Model Inspector+). The modal composition of sandstones in thin section was determined using a Swift Model J point counter (n=300), following Dickinson and Suczek (1979) and Dickinson et al. (1983). The composition of fine-grained sandstone matrix was determined using a PDF-2 X-ray powder diffractometer at the Department of Geological Sciences, FU Berlin.

Stratigraphy

Lithological units of the western Dycedale Syncline ca. 500 m thick are nearly continuously exposed in fresh and weathered roadcuts along the R40 paved road where the trend of bedding obliquely intersects the road, and are also adequately exposed in grasslands nearby (Figures 3, 4). They are crosscut by several dykes of intermediate to mafic composition, which form part of an extensive, regional, dominantly south-southeast to north-northwest-trending dyke set (Figure 3). While there are clearly several generations of dykes and multiple cross-cutting relationships, the major part of the dyke swarms is thought to represent feeders to the Nsuze Group of the Pongola Supergroup. A dyke near Barberton was dated at ~ 2967 ± 1 Ma (Olsson et al., 2010).

The stratigraphic base (Figure 5) is dominated by fine- to medium-grained sandstone (unit A) >100 m thick, overlain by ca. 40 m of polymict conglomerate (B), which fines upward into ~30 m interbedded clast- and sand-matrix-supported conglomerate and gravelly sandstones (C); these include large fragments of microbial mats. The contact with the overlying unit D, a ~40 m-thick, medium- to coarse-grained, horizontally and cross-

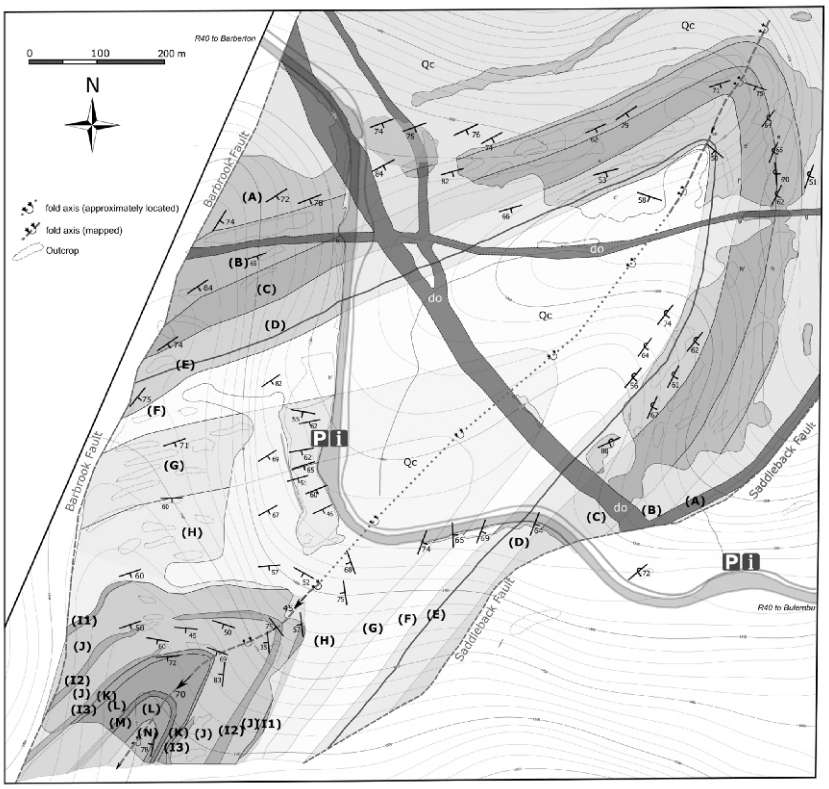

Figure 3. *Detailed geologic map of the western Dycedale Syncline, modified from Bläsing et al. (2015). A-N: stratigraphic units discussed in text; do = dolerite dyke; Qc = Quaternary cover.*

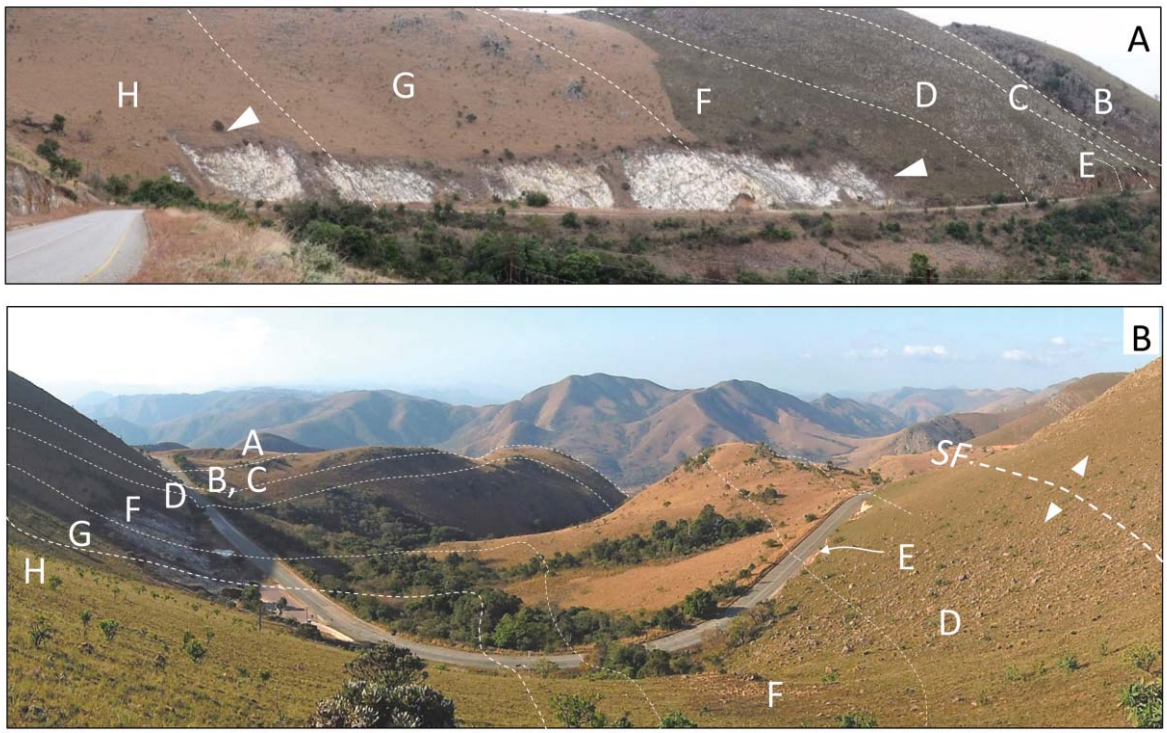

Figure 4. *Geomorphology of Moodies Group strata in the westernmost Dycedale Syncline. White triangles mark facing direction, capital letters denote stratigraphic units. (**A**) View of the northern limb towards the west, including "White Outcrops" which expose >200 m of stratigraphic section. (**B**) View up-plunge towards the northeast of the western Dycedale Syncline, illustrating the well-exposed northern (left) and overturned southeastern (right) limb of the syncline, cut by the ravine in the center middleground. "White Outcrops" are located in the shade to the left. SF = Saddleback Fault.*

bedded sandstone with desiccation cracks on shale partings and abundant rip-up clasts, is sharp. Its upper part includes a thin andesitic lava flow (E). The overlying tripartite tuffaceous sandstone (F, G, H) reaches about 230 m in thickness. It shows, best exposed in the "White Outcrops" along the R40 road, cross stratification, rip-up clasts, mud-coated ripples, exposure surfaces, desiccation cracks, silicified gypsum clasts and single-clast-thick conglomerate. Unit H is overlain by gravelly sandstone about 65 m thick (J), interrupted by three wedge-shaped conglomerates (I1 to I3). The uppermost preserved units include laminated magnetic shale (K) and two flow units of basaltic lava (L), separated by siltstone with thin jaspilite bands (M) and overlain by tuffaceous shale and siltstone (N). All units are described in detail in Table 1 and in associated figures (Figures 6 to 11).

Sedimentary architecture and lithology suggest that the basaltic lava flows (L) correlate with the most prominent marker unit in the Moodies Group, the Moodies Basaltic Lava (unit MdL2 of Visser et al., 1956, and of Anhaeusser, 1976).

Paleocurrents

The dip direction of several hundred foresets was measured at thirteen sites in the study area, corrected for the plunge of the synclinal axis (mean value 210/57°) and unfolded. The orientation of dominant sediment transport is displayed in rose diagrams (Figure 5) by stratigraphic unit. Limited data from unit A indicate bidirectional transport, possibly an artefact of outcrop exposure of the subvertical beds. Foresets in sand lenses within the conglomerates of unit B and in gravelly sandstones of unit C indicate a dominant southwesterly transport. The overlying shoreline-facies unit D and lower part of the intertidal-facies unit F, G and H record mostly north-directed transport. On the overturned limb, units D and F show a bidirectional component dominated by a south- and southwestward transport direction, approximately parallel to the strike of the belt.

Petrography

Matrix-poor Moodies sandstones in the Dycedale Syncline are largely arkoses and subarkoses (Figure 12). Matrix-rich sandstones classify as volcanolithic wackes. Care has to be taken in these rocks to correctly interpret metamorphically altered grains (Heubeck and Lowe, 1999).

Principal framework components include monocrystalline quartz (some of it water-clear and showing resolution embayments, indicating a volcanic origin), polycrystalline quartz and a variety of cherts, including organic-rich (black), organic-poor (grey), and ferruginous (red) chert. Monocrystalline quartz can occasionally be observed to be intergrown with feldspar, und thus be identified as plutonic. Polycrystalline quartz grains with aligned sutured domains, suggesting a metamorphic provenance, were not observed. Grain-scale textures, such as lamination, flow banding or shard outlines, lapilli fragments, microbreccias, and microcrystalline vein quartz demonstrate that a variety of silicified volcanic rocks contributed to generate quartzose components. Abundant orthoclase and common microcline make up the high feldspar content, reaching up to 30%. Plagioclase was not observed. In some beds, feldspar is fresh (Figure 13A). Nodules, common in units D through G, are inclusion-rich but pervasively silicified. In thin section, they show the characteristic, strongly undulose extinction and subgrain development of gypsum (Nabhan et al., 2016a; Figure 13B).

Several types of sediments and volcanics were reworked into sedimentary matrix. These include shale fragments (Figure 13C), which are clearly derived from soft (where wispy) or mudcracked (where angular and blocky) shale, evenly fine-grained, light-colored tuff clasts lacking internal textures (Figure 13D) and quartz-sericite-mosaic (QSM) grains. The latter were interpreted by Heubeck and Lowe (1999) to represent altered (sub-) volcanic rocks. The quartz content in this grain type is highly variable so that its composition ranges from sericite-bearing chert to massive sericite grains.

Sandstone cement consists of a mixture of very-fine-grained impure chert, sericite, and carbonate. The degree of compaction is variable and is highest in matrix-rich sandstones; in contrast, matrix-poor sandstones, best developed in unit C, show well-preserved open interstices and a higher percentage of grain-to-grain point contacts. Grains are largely subangular to subrounded; the degree of sorting is highly variable.

Discussion

Depositional environments

A fluvial-to-tidal transition

Excellent sections of fluvial-to-tidal transitions are exposed on both limbs of the syncline. A partial section from the overturned limb was described by Eriksson et al. (2006), who pointed out the unusual combination of alluvial braidplain and estuarine tidal facies. They explained this combination by the lack of channel-confining vegetation, which aided avulsion, active tectonism, and to a high tidal range. Our study supports this model but adds detail from the section on the normal limb of the syncline, which is more complete, thicker, better exposed, and more readily accessible.

The overall succession is transgressive, with fluvial deposits at the base, overlain by coastal and tidal-estuarine deposits, prior to the reestablishment of shallow-coastal and alluvial conditions, indicated by the three conglomerate units I1 - I3 and the fine-grained units K, M and N. An interpretation as a tide-dominated delta (Eriksson, 1979) would require an overall regressive / progradational sequence that is not observed here. In addition, the evidence of slack-water deposition places the overall depositional environment inshore, that is, within an estuary of some sort because slack-water does not develop in offshore tidal areas so that mud does not settle there and is diluted too quickly (Allen, 1991; Dalrymple and Rhodes, 1995).

Evidence of widespread tidal action consists of (1) rhythmic high- and low-energy deposition, evidenced by cross-bedded sandstone combined with shale drapes; (2) evidence of periodic desiccation between periods of flooding; and (3) the early diagenetic formation of (now silicified) evaporitic nodules (Nabhan et al., 2016a) in the vadose zone of water-lain sediment. The numerous but thin shales and tuffites show that periods of

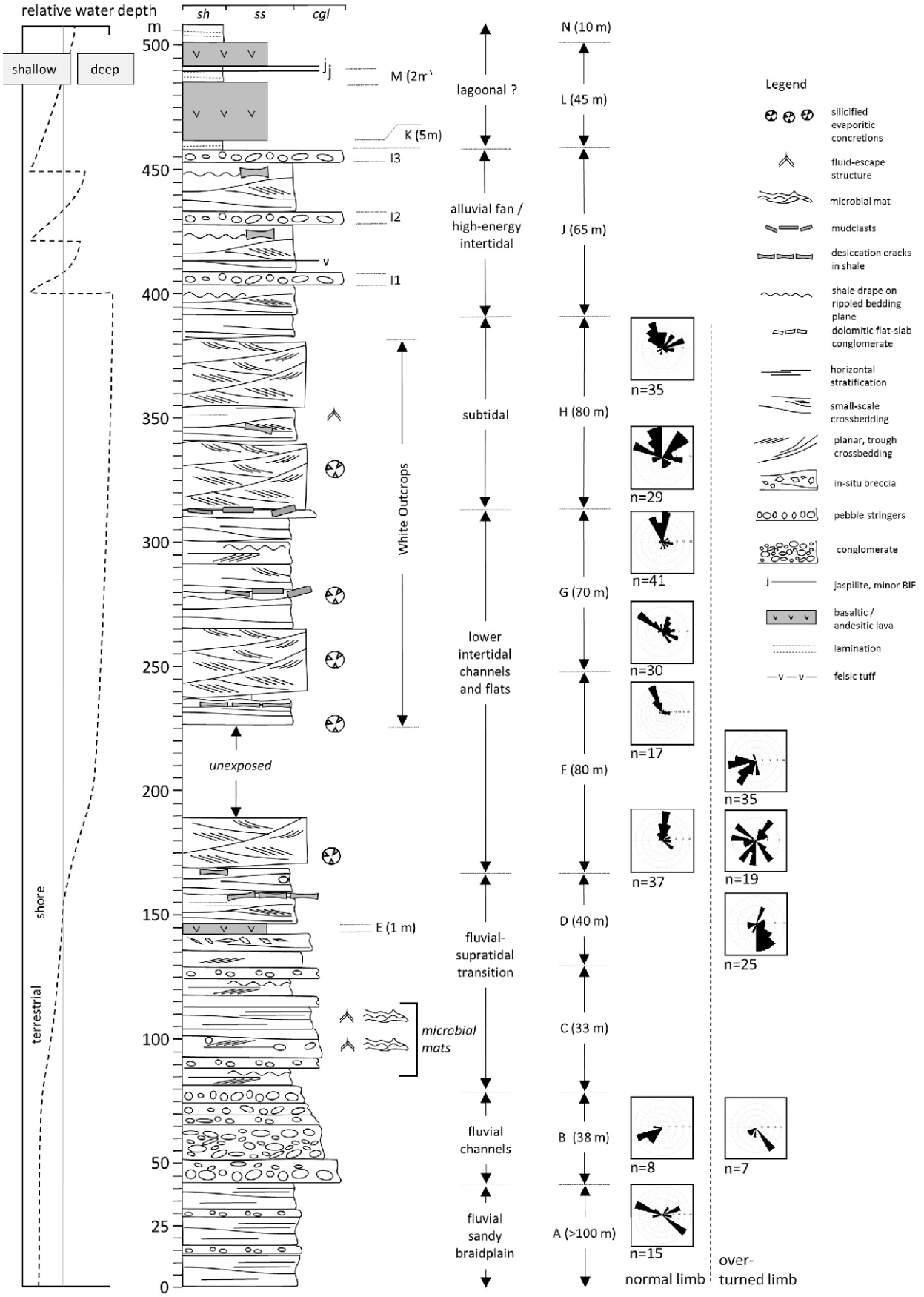

Figure 5. *Stratigraphic column of Moodies strata in the western Dycedale Syncline, measured along the normal limb.*

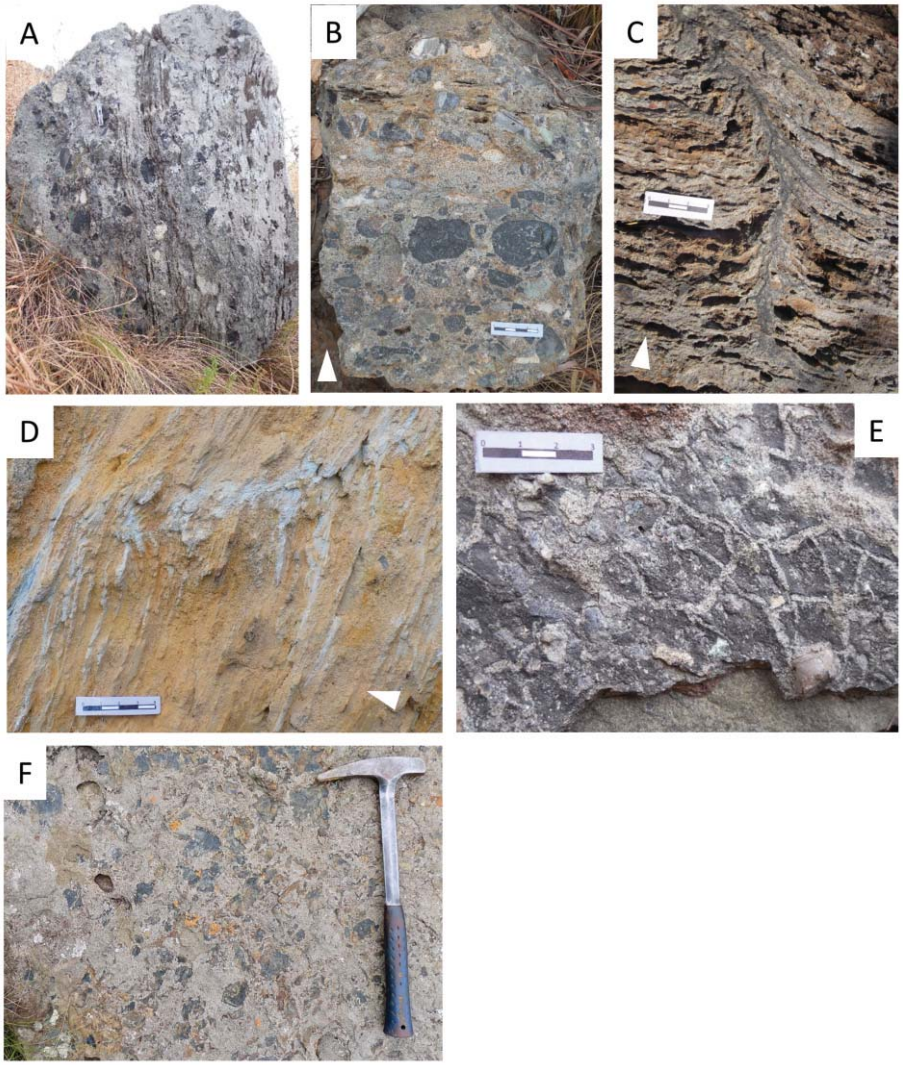

Figure 6. *Sedimentary structures in units A-C. White arrowtips indicate stratigraphic-up direction.* ***(A)*** *Thick-bedded, matrix-supported conglomerate interbedded with laminated microbial mats (center); unit B.* ***(B)*** *Close-up photograph of poorly sorted chert-clast conglomerate; microbial mat near top; unit B.* ***(C)*** *Fluid-escape structure in biolaminated sandstone; unit C.* ***(D)*** *Fluid-escape structure in weathered, biolaminated sandstone, unit C; R40 roadside outcrop.* ***(E)*** *Desiccation cracks in shale coatings interbedded with conglomerates, unit A.* ***(F)*** *Sand-matrix-supported mud-chip conglomerate, unit A.*

slack current were frequent but short, considering the high proportion of suspended matter incorporated in sandstone, not in mudstone.

Clearly, most of the time, the depositional environment was dominated by vigorous currents. Nevertheless, the beds show transitions from tuff-clast-rich viscous debris flows to matrix-rich wacke and to matrix-poor crossbedded subarkoses and sublitharenites with fresh K-feldspars. This small-scale variability argues that the fine-grained tuffaceous matrix affected deposition and is therefore largely primary, not a local product of hydrothermal breakdown of unstable lithic grains. The resulting flow may have resembled at times and locally a low-density slurry in which – despite basal shear stress high enough to create mid-sized aqueous dunes - turbulence was insufficient to keep all volcanic ash in suspension. The high fallout rate of tuffaceous material may have hindered grain saltation and bedload transport through increased viscosity.

The stacking pattern of high- and low-energy deposition in units F through H, combined with bedforms oriented by changing flow directions, allows an interpretation of specific flow conditions (Martinius and van den Berg, 2011): The dominantly unidirectional transport direction, combined with rare but periodic slackwater deposition, can be ascribed to fluctuations in fluvial discharge and resulting tidal influence; these are characteristic for the fluvial-tidal transition zone (Figure 14A, B; Dalrymple and Choi, 2007). In such a setting, the thick crossbeds are created during high fluvial discharge, whereas the horizontal beds with single (in the intertidal zone) or double (in the subtidal zone) mud drapes bounded by reactivation surfaces are generated by the intruding flood tide at low fluvial discharge. Possibly, shale drapes were also deposited in ponds at low slack tide because suspended sediment was abundantly available (Fenies et al., 1999).

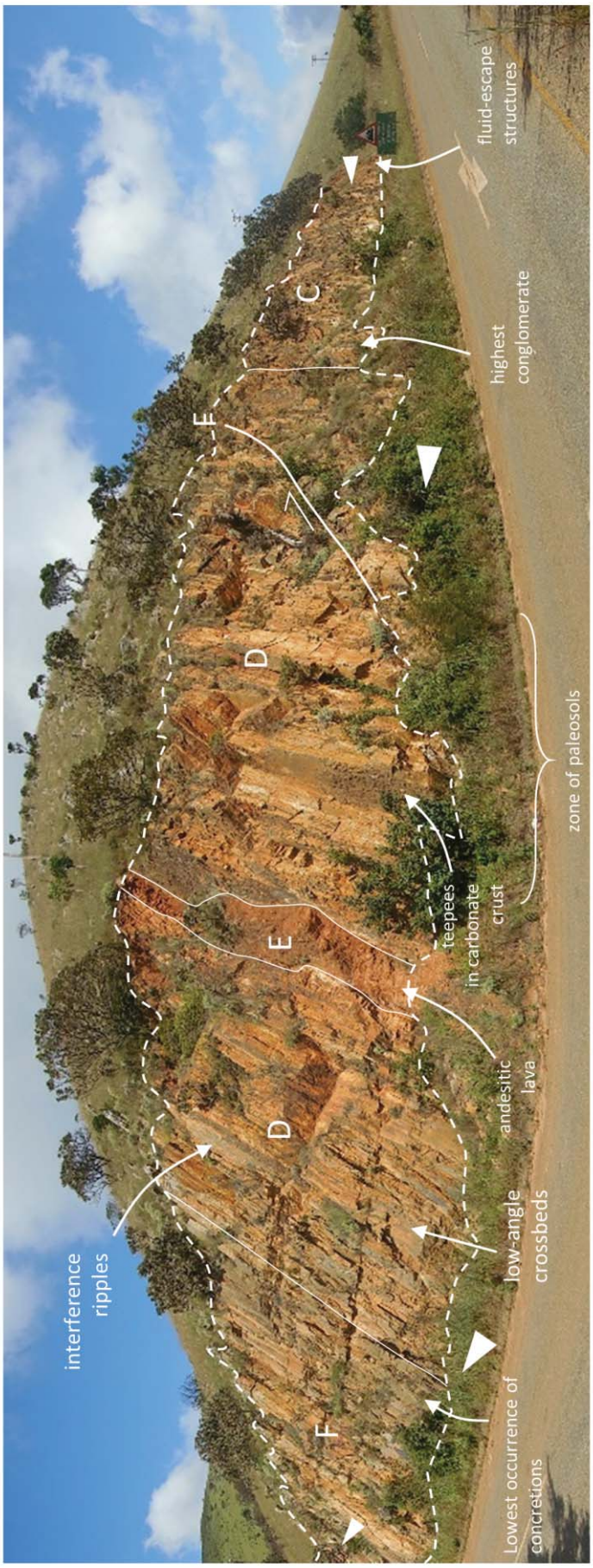

***Figure 7**. Panorama photograph of the fluvial-to-tidal transition exposed in the R40 roadcut on the normal (northern) limb of the Dycedale Syncline. Stratigraphic top is to the left. See text for description.*

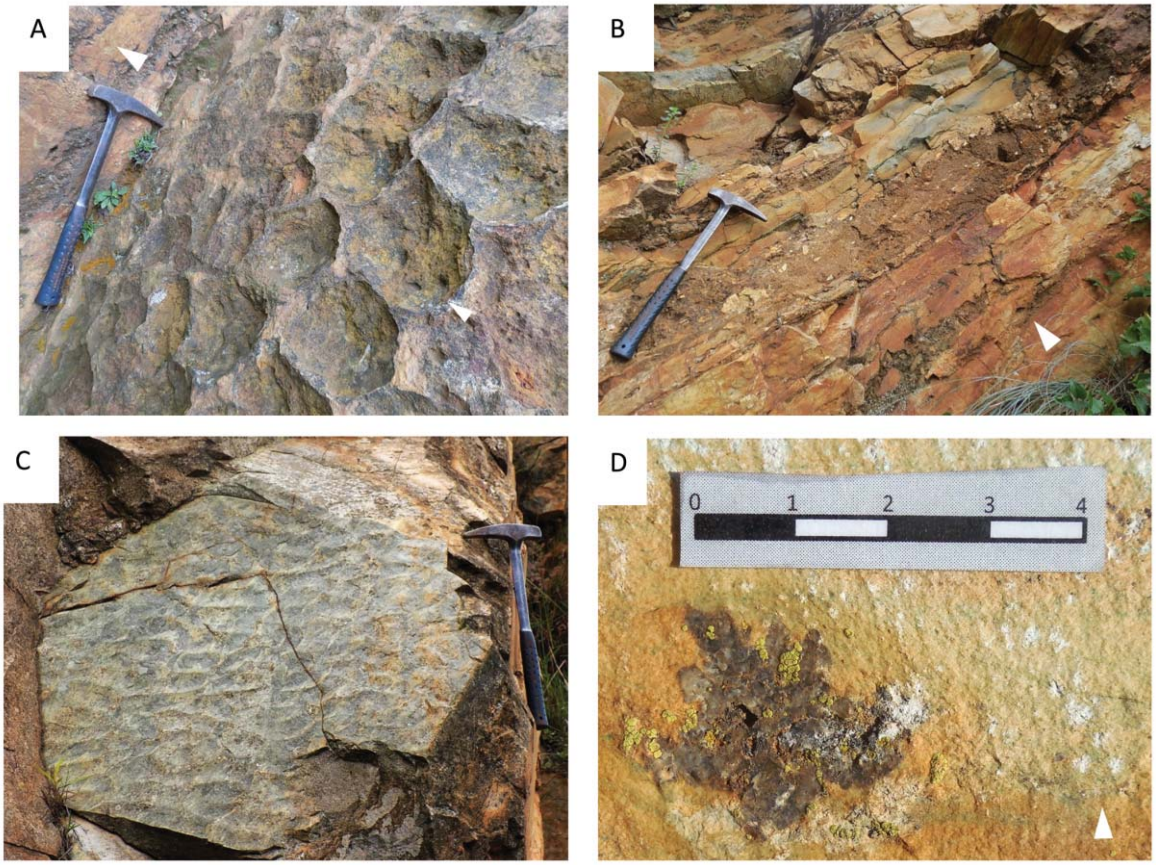

Figure 8. *Sedimentary structures in unit D and basal unit F of the roadside outcrop shown in Figure 7.* ***(A)*** *Oblique view of pseudopolygonal teepee ridges in dolomitic duricrust.* ***(B)*** *Cross-sectional view of very poorly sorted nodular sandstone with abundant duricrust fragments.* ***(C)*** *Top-down view of prominent south-dipping bedding plane with shale-coated interference ripples; some of them mudcracked.* ***(D)*** *Radial cluster of early diagenetic transparent prismatic crystals in horizontally bedded, tuffaceous silty sandstone of basal unit F; R40 roadside outcrop.*

Sedimentation rates were likely high, balanced by equally high subsidence rates. Such an inference is supported by the stacking of >200 m of stratigraphic section between the base of unit F and the middle of unit H with apparently only minor changes in hydrodynamic conditions; any available accommodation space was apparently readily filled by sediment which underwent little reworking. It thus stands to reason that units exposed in the "White Outcrops" (and possibly also in the over- and underlying units) constitute a very-high-resolution time record.

Paleocurrent rose diagrams from units F- H (Figure 5) shows only a weak bidirectionality. Most rose plots have a strong unidirectional component. This may represent the commonly observed pattern of flood and ebb currents occupying separate tidal channels (Allen, 1991; Nio and Yang, 1991; Dalrymple and Rhodes, 1995) or flow in shallow channels and in intertidal areas of filled estuaries (Figure 14A, B). Deep channels, in contrast, are flooded both by ebb and flood currents and thus may show well-developed, oppositely directed herringbone cross-stratification (Figure 14C). However, local changes in channel morphology and the fluvial-tidal transition zone also allow herringbone cross stratification to form (Dalrymple and Choi, 2007; Martinius and van den Berg, 2011).

Water depth and tidal range

The approximate water depth in which the subaqueous dunes of units F, G, and H formed can be calculated following Leclair and Bridge (2001), who estimate the mean preserved set thickness to be approximately one-third the height of the original dunes (h_m). The mean 6.9 cm preserved thickness from 163 measured foreset heights in the White Outcrops (Table 2) thus corresponds to h_m = ca. 0.2 m. Paleo-water depth (d, in m) is then approximately $3< (d/h_m) <20$ m; thus, $0.6< d <4$ m. Because this equation was developed for cross beds formed in fluvial environments, it may not be accurate for tidal settings but must serve as a rough estimate only. If dunes of units F through H widely formed in water depths between 0.5 and 4 m, their association with mudcracked shale would indicate approximately a mesotidal range. This would allow occasional exposure of tidal channels and frequent widespread exposure of tidal flats, which would in turn favor the early diagenetic formation of the nodules in the upper intertidal and supratidal zone.

It is problematic to generalize from the findings of a single outcrop to Archean global tidal processes. Because the Moon-Earth distance was reduced and Earth spun faster, Archean tides are thought to have been high-amplitude and somewhat more frequent within one solar day (sunrise to sunrise) in comparison

Table 1. Stratigraphic units in the western Dycedale Syncline.

Unit Name	Thickness (m)	Principal Lithology	Subordinate Lithology	Location and Exposure	(Sedimentary) Structures	Internal Organization	External Geometry	Processes	Depositional Environment
N	10	• siltstone, olive, tuffaceous		core of syncline	• laminated			• low-energy flow, sedimentation dominated by suspension settling	protected terrestrial or coastal setting (lagoonal, bay)
M	2	• jaspilite, impure		core of syncline	• laminated			• low-energy flow, sedimentation dominated by suspension settling	protected terrestrial or coastal setting (lagoonal, bay)
L	45	• basaltic lava		core of syncline	• amygdaloidal			• subaerial or shallow aquatic lava flow	protected shallow-water setting inferred from adjacent units
K	5	• shale, olive-grey to black, magnetic		core of syncline	• banded or laminated			• low-energy flow, sedimentation dominated by suspension settling	protected terrestrial or coastal setting (lagoonal, bay)
J	65	• sandstone, gravelly, medium-bedded, coarse-grained, tuffaceous	• shale, green and offwhite, tuffaceous, with nodule clusters		• horizontally stratified			• strong currents sufficient to transport tuff slabs and gravel and to vigorously rework the substrate	high-energy tidal system fringed by alluvial fans
			• abundant tuff fragments clasts up to 20 cm * 3 cm		• cross-bedded			• occasional slack water	
			• one discontinuous bed of volcanic tuff					• subaerial exposure and upward-directed groundwater flow	
I1 I2 I3	2-4 (each)	• chert-cobble conglomerate, matrix-poor		adjacent to Barbrook Fault (Figure 3)	• clast imbrication	• normally graded, clast-supported	• wedge-shaped	• intermittent very-high-energy events of low flow depth	steep small alluvial fans
					• max. clast size 28 cm * 40 cm	• top of units fine rapidly	• erosive base		
H	80	• sandstone, offwhite, medium- to fine-grained	• rare tuffaceous shale	"White Outcrops" (south) (Figure 4A)	• abundant planar and trough crossbedding (Figure 14C)	• rare fluid-escape and load structures in the upper part of the unit	• gradational contact to underlying unit G	• rhythmic mix of deposition from bed- and saltation load with suspension load	subtidal estuarine channel
		• variably tuffaceous and in places gravelly	• common clasts of tuffaceous material, granules of black chert		• rippled bedding planes			• moderately fast unidirectional flow	
		• grading into tuffaceous wacke	• angular or wispy, light-green shale fragments		• shale drapes			• subaqueous setting of high sedimentation rates	

Table 1. Stratigraphic units in the western Dycedale Syncline. *(continued)*

Unit Name	Thickness (m)	Principal Lithology	Subordinate Lithology	Location and Exposure	(Sedimentary) Structures	Internal Organization	External Geometry	Processes	Depositional Environment
G	ca. 70	• sandstone, offwhite, medium- to fine-grained	• abundant tuffaceous sediment as drapes, as (semi-) indurated clasts, and as matrix	"White Outcrops" (center) (Figure 4A)	• abundant planar and trough crossbedding (Figure 14B)		• gradational contacts at base and top	• dominant current flow of variable, mostly moderate strength	intertidal; similar to underlying unit F
		• variably tuffaceous and in places gravelly			• rippled bedding planes		• top of unit drawn at a 30 cm thick tuffaceous, clast-bearing sandy debris flow	• erosion of semiconsolidated and tuffaceous sediment with evaporitic nodules from bank channel margins	
		• grading into tuffaceous wacke			• variety of clast types, including silicified gypsum nodules (Figure 10C and D)			• some standing water	
					• very rare desiccation cracks			• rare subaerial exposure	
F	ca. 80	• sandstone, offwhite, matrix-rich, medium- to fine-grained	• shale partings and drapes (Figure 10B)	"White Outcrops" (north) (Figure 4A)	• abundant trough and planar cross-beds 3-12 cm thick (Figure 10A, 14A).	• shale drapes are laterally truncated within a few m	• gradational contact to overlying unit G	• rhythmic mix of deposition from bed- and saltation load with suspension load	network of wide and shallow estuary channels eroding a mosaic of subaerially exposed arid inter- to supratidal flats and coastal sandplains with siliciclastic, volcanic, and evaporitic components, topped by dolocrete paleosols and protected shallow ponds
		• variably tuffaceous and in places gravelly			• Straight-crested ripples of variable asymmetry and wavelengths of ~ 3 to 3.5 cm with common green mud drapes	• desiccation cracks decrease upsection	• top of unit drawn at a thick dark green shale bed	• reversing currents of considerable strength	
		• grading into tuffaceous wacke			• common desiccation cracks			• occasional subaerial exposure	
					• in places abundant *in-situ* (solitary, concatenated, clusters) or reworked silicified nodules up to 5 cm in diameter (Figure 10C, D)			• moderate degree of erosion	
					• common intrabasinal clasts (angular or wispy shale, tuffaceous sandstone, orange carbonate); rare extrabasinal chert clasts (Figure 11)				

Table 1. Stratigraphic units in the western Dycedale Syncline. *(continued)*

Unit Name	Thickness (m)	Principal Lithology	Subordinate Lithology	Location and Exposure	(Sedimentary) Structures	Internal Organization	External Geometry	Processes	Depositional Environment
E	ca. 0 - 1	• andesitic lava		midsection in unit D on both limbs (Figures 5, 7)	• randomly oriented offwhite acicular crystals in fine-grained matrix (Figure 9A)	• spheroidal weathering	• top appears shallowly eroded by low-angle cross-bedded sandstone (Figure 9C)	• surface lava flow	
						• white elongate tuffaceous wisps of dm-size near base (Figure 9B)	• base concordant with underlying sandstones (Figure 9B)		
D	40	• sandstone, pebbly, medium-grained, well-sorted	• minor discontinuous strings of pebbly sandstone	excellent outcrops along R40 road (Figure 7)	• medium- to thinbedded, dominantly horizontally stratified and low-angle cross-stratified	• upsection decrease in proportion and thickness of pebbly sandstone and of clast size	• top at the highest documented pebble	• abundant sand transport at moderate to slow currents, rarely sufficient to transport gravel	shallow braided streams transiting into an extensive, probably supratidal sand flat environment, coastal bay or lagoon, bayhead
			• shale partings and drapes common towards the top of unit (Figure 8C)		• prominent tilted bedding plane along R40 road exposes pseudopolygonal carbonate crust (Figure 8A)	• on overturned limb, widespread shale-chip conglomerate and shale-clast-laden megaripples		• occasional rapid flooding of shallow or desiccated shaly ponds; reworking	
			• several diamictites (interpreted as regoliths and paleosols) (Figure 8B)		• nodules, dissolution features and mottled patchy discoloration in several diamictites, each bed 20 to 50 cm thick (Figure 8B)	• upsection increase in linearly arranged, hollow-cored, crystal-lined nodules along bedding planes and foresets		• early diagenetic formation of duricrusts and calcareous and sulfatic nodules in the vadose zone in subaerial settings under conditions of upward-directed groundwater flow	
					• prominent tilted bedding plane along R40 road exposes desiccated shale drape (Figure 8C); rare rip-up shale clasts (Figure 8D)				
C	33	• sandstone and conglomerate, pebbly, medium-grained	• *in-situ* carbonaceous microbial mats, <1 mm thick, mm-spaced, dark greenish, planar to moderately wavy-crinkly	excellent outcrops along R40 road (Figure 7) and on ridge of northern limb (Figure 3)	• horizontal lamination and crossbedding in sandstone		• top of unit at highest occurrence of conglomerates	• growth of microbial mats in a subaerial setting where they were exposed to very-high-energy, episodic floods	terrestrial floodplain landward of the intertidal zone
			• microbial-mat conglomerate		• tufts, complex bulbous domes, thick coherent laminae			• delayed dewatering due to impermeable microbial mats; possibly fluctuating groundwater	

Table 1. Stratigraphic units in the western Dycedale Syncline. *(continued)*

Unit Name	Thickness (m)	Principal Lithology	Subordinate Lithology	Location and Exposure	(Sedimentary) Structures	Internal Organization	External Geometry	Processes	Depositional Environment
C *continued*	33		• rare patches of mudstone		• linear dewatering structures (Figure 6C, D) • desiccation cracks in mudstones			• high sedimentation rates • limited quiescent conditions	
B	38	• cobble conglomerate, thickbedded; well rounded but poorly sorted (Figure 6A, B)	• lenses of coarse-grained gravelly sandstone	excellent outcrops along R40 road (Figure 4A) and on ridge of northern limb (Figure 4B)	• horizontal clast alignment (Figure 6A, B) • abundant clast imbrication (Figure 6A, B) • upper-plane-bed horizontal stratification	• fining- and thinning-upward (1 m at base; ca. 5 cm near top) • high degree of downcutting • lateral pinchout within tens of m	• gradual but rapid transition at base • top at uppermost cgl	• bedload transport of clasts • turbulent transport of saltating sand • subaerial transport inferred from adjacent units	high-energy braided-stream with poorly defined, wide and shallow channels between migrating bars
A	>100	• sandstone, medium- to coarse-grained, quartz-and carbonate-cemented	• dark grey mud-chip sandstone and mudchip-conglomerate (Figure 6F) • tan-colored tuff fragments and isolated chert pebbles, commonly organized in single-clast-thick stringers	poorly exposed on northern limb on north-facing grassy slopes (Figure 3)	• abundant horizontal bedding, some low-angle planar crossbeds in thin sets • desiccation cracks (Figure 6E) • laterally erosive within tens of m; no deep channelization			• frequent and unsystematic variations in flow strength within a setting of moderate to high current velocity • occasional local desiccation of standing-water pools in subaerial settings	sandy fluvial floodplain

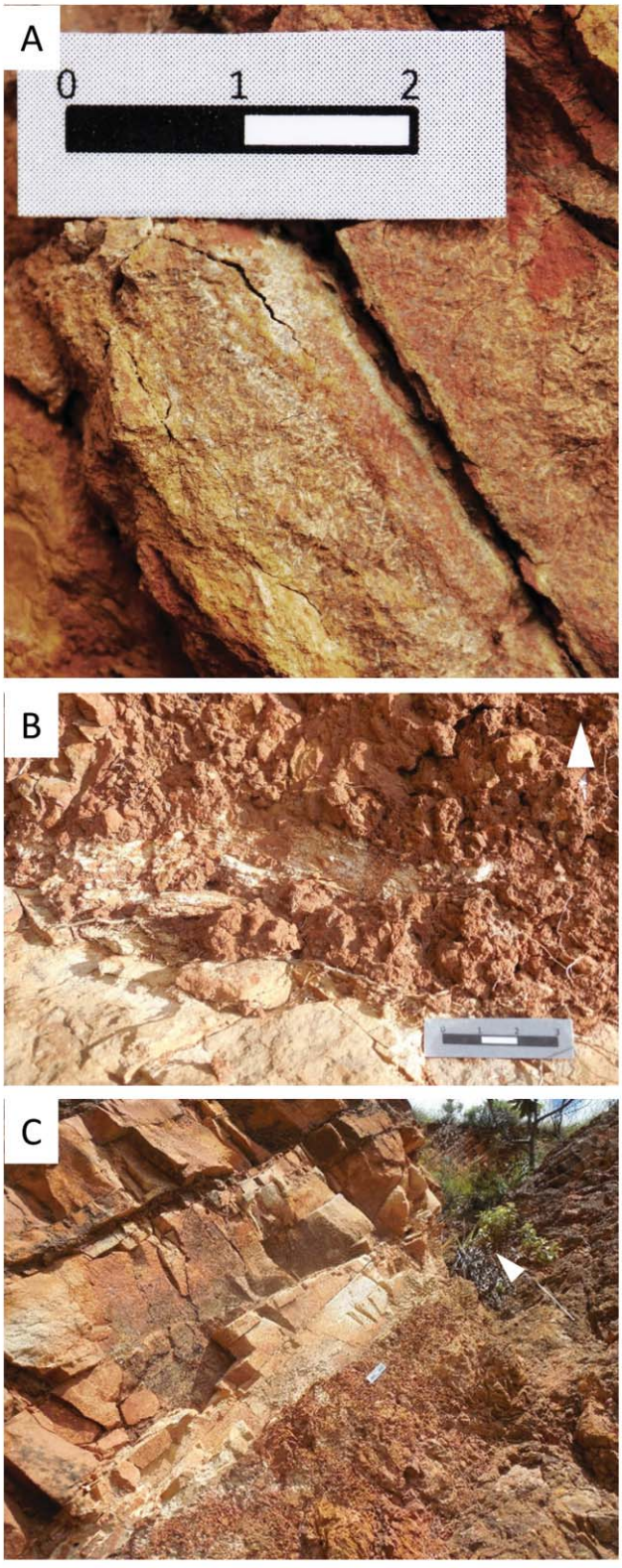

Figure 9. *Weathered andesitic lava (unit E); see Figure 7 for location. (**A**) White, random-oriented acicular crystals, likely plagioclase, in fine-grained matrix; (**B**) basal section of lava (weathering crumbly and orange) showing a white, elongate, probably tuffaceous rip-up clast overlying low-angle-cross-bedded sandstone; (**C**) erosional top of the flow, overlain by low-angle cross-bedded sandstone.*

to recent tides (Williams, 2000; Mazumder and Arima, 2005; Coughenour et al., 2009). This inference is consistent with a disproportionally high percentage of tidal deposits in the Archean stratigraphic record (Eriksson et al., 2004). However, the preserved record may not be globally representative, and the observation of recent tidal dynamics teaches us that the amplitude of recent tides (and thus the local stratigraphic architecture) is largely locally controlled by shelf bathymetry and coastline morphology, not by first-order Earth-Moon dynamics. Thus, an interpretation of Archean tidal sandstones in terms of high tidal ranges and short periods may be attractive (e.g., Eriksson and Simpson, 2002) but not be warranted.

Could Moodies tidal deposits represent hypertidal (>6 m) amplitudes? Recent hypertidal regimes are rare (Eisma, 1997; Archer, 2013). They show very large twice-daily differences in water depth and rhythmic suspension-settled and bedload-transported sediments (rhythmites). In such settings, very large areas repeatedly fall dry and are re-flooded, generating superimposed dune, ripple and laminae-scale features that are indicative of deep-, then shallow-water flow followed by emergent runoff from bedforms that were rapid-flow, deeply submerged only hours before. Because tides advancing and retreating over wide flat areas may take the form of highly turbulent bores (essentially long-distance-migrating breakers), the degree of turbulent reworking may be high. Because the water column continuously loads and unloads un- and semiconsolidated sediment at high rates, fluid-escape structures tend to be common (Archer, 2013). Because high current velocities are dominant, mud accumulates only during brief slack tides and in distant settings of significant water depth if it is not washed out to the deep sea (van den Berg et al., 2007; Martinius and van den Berg, 2011).

Even though Units F, G, and H in the western Dycedale Syncline all show some sedimentary structures that conform to the above-listed processes, it is probably impossible to accurately quantify tidal range from these outcrops. Attempts at quantifying tidal parameters even in Phanerozoic cases are fraught with uncertainty (e.g., Archer, 1996; Coughenour et al., 2009). In addition, even if Dycedale Syncline strata had been deposited under hypertidal conditions, their global representativeness cannot be assumed. Rather, the inferred Moodies paleogeography in elongate basins between rising granitoid plutons may have amplified the tidal range. Thus, whether the tidal setting indicated by Moodies Group strata is a local / regional effect or an expression of the Archean Earth-Moon system remains unknown.

Evaporitic nodules

Early diagenetic nodules composed of silicified gypsum are common in the Moodies Group at several stratigraphic levels and in nearly all Moodies tectonic blocks north of the Inyoka Fault (Nabhan et al., 2016a). They count among the oldest terrestrial evaporites known to date and among the oldest-known compound paleosols. Nabhan et al. (2016a) documented excellent occurrences from lower Moodies strata in the eastern Stolzburg Syncline, ca. 20 km to the west and stratigraphically ca.

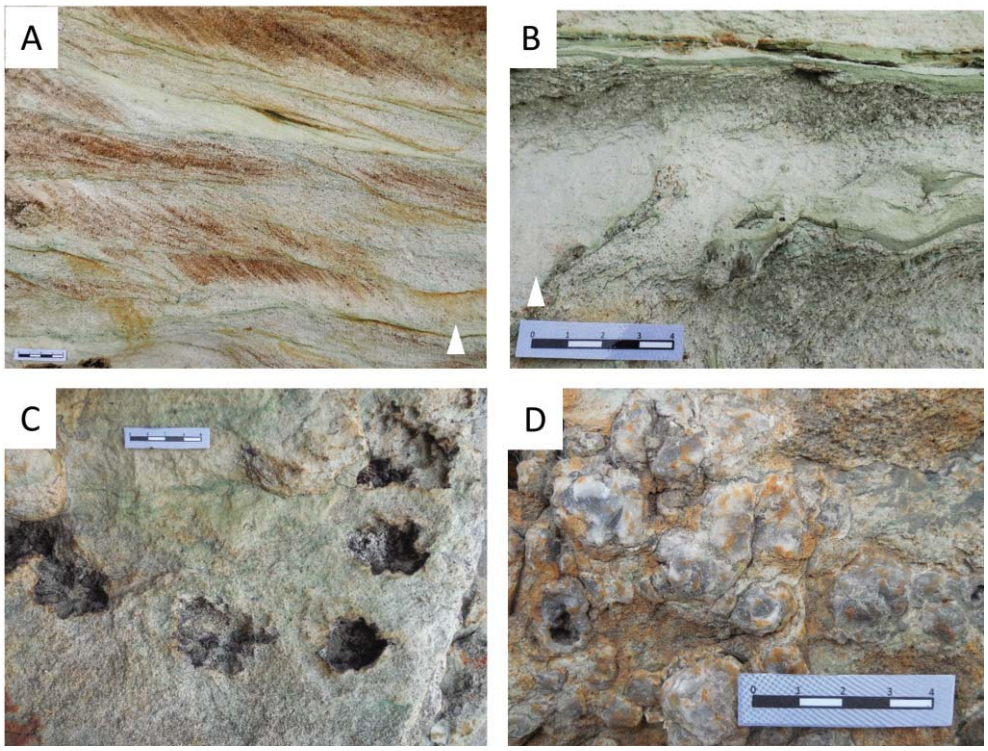

Figure 10. *Sedimentary structures in units F and G of "White Outcrops" location. (**A**) Typical ripple-drift cross-laminated sandstone. Cross-beds are dominantly inclined to the right, indicating an overall southwesterly transport direction. (**B**) Green shale drape (top) and soft shale clast (below) in white, tuffaceous-matrix-rich sandstone. (**C**) Top-down view on a bedding plane showing hollow angular cavities which outline radially-outward-grown nodular crystal clusters. (**D**) Top-down view on a bedding plane showing clustered, largely chert-filled nodules. The hollow nodule is chert-lined.*

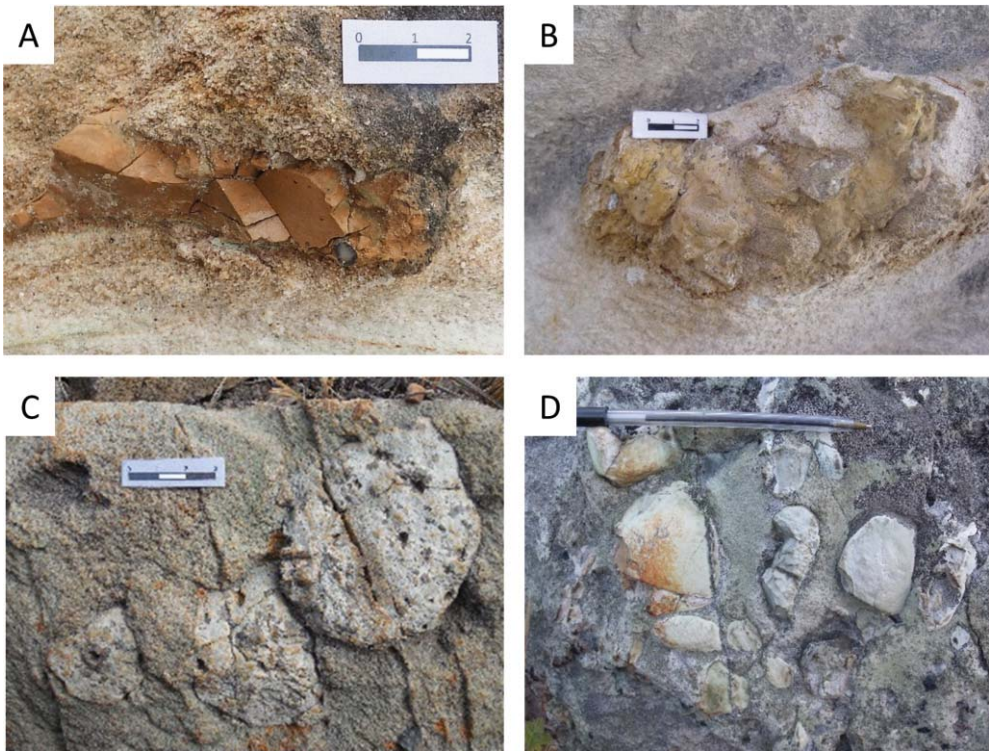

Figure 11. *Clast types in tuffaceous cross-bedded sandstones (Unit G) at the "White Outcrops" location. (**A**) Indurated, orange, fine-grained, calcareous and tuffaceous clast lacking stratification, possibly eroded from a dolomite duricrust such as exposed in Unit D. (**B**) Clast composed of rounded clumps of sandstone in a yellow tuffaceous matrix. Poor sorting and lack of stratification suggest indurated debris flow or paleosol provenance. (**C**) Cluster of well-rounded feldspar-porphyry clasts with large idiomorphic quartz crystals in sandy matrix. (**D**) Cluster of well-rounded tuff clasts lacking xenocrysts. Pen for scale is 14 cm long.*

1000 m lower than the Moodies strata of the Dycedale Syncline, but they also occur here in units D to G, placed in a similar braided-fluvial to supratidal depositional setting. Nabhan et al. (2016a) interpreted the nodules as having formed during early diagenesis within unconsolidated granular sediment in the vadose zone, which was affected by seasonal or tidal groundwater level fluctuations.

The nodules are largely silicified, consisting of pseudomorphs of megaquartz after gypsum, barite and calcite. Electron microprobe mapping shows the rare presence of anhydrite, barite and calcite. The nodules formed through the weathering of tuffaceous material and feldspar which delivered alkali cations such as Ca, Ba, and K. Carbonates were likely supplied by silicate weathering of mafic to ultramafic volcanic rocks. Even though sulfate was generally low in Archean oceans (Habicht and Canfield, 1996), terrestrial brines, in particular in coastal zones, probably had elevated sulfate concentrations because sulfate was delivered there by oxidative pyrite dissolution. Oxygen, in turn, may have been supplied to the pore space (but not to the atmosphere) by nearby photosynthetic microbial mats (Homann et al., 2015).

Many nodules in unit G of the Dycedale Syncline show radially-inward-directed crystal growth and commonly hollow interiors. Nabhan et al. (2016a) explained this texture by an early diagenetic partial silicification of the nodules which stabilized and protected their rims from dissolution; alternatively, microbial sulfate reduction of the gypsum surfaces to carbonate would had have the same effect. Evidence for such microbial involvement comes from isotopically depleted ($\delta^{34}S$ < -20‰) detrital pyrite overgrowths in heavy mineral laminations adjacent to the nodules (Nabhan et al., 2016b).

Depositional setting of lava and of jaspilite units

Depositional settings of the highest stratigraphic units in the Dycedale Syncline, including the basaltic lava (unit L or MdL2) and associated ferruginous sediments, cannot be inferred with certainty from outcrops in the Dycedale Syncline. Laterally extensive exposures of these units in the Saddleback and Eureka Syncline have not been well investigated to date. Nowhere in the BGB have pillow structures or load structures, indicative of subaqueous extrusion, been found, nor is there unambiguous evidence of surficial Archean weathering of the lava.

The lava is commonly interbedded with siltstone and (bio-) chemically precipitated jaspilite (Kappler et al., 2005) and is over- and underlain by thick units interpreted to represent fluvial, coastal-pond, and even alluvial facies (Heubeck and Lowe, 1994a; Bläsing, 2015). It is thus reasonable to assume that the lava flooded, over its 60 km outcrop width, a range of coastal environments. In the Dycedale area, this included a shallow-water setting of fluctuating depositional energy, perhaps a lagoon or bay near the base of alluvial fans.

Table 2. Measured thicknesses of foresets from units F and G of the "White Outcrops"

unit	n=	h(cm)	σ
F	68	7.2	3.4
G	45	6.9	2.7
G	30	6.4	2.6
top G	20	6.8	2.1

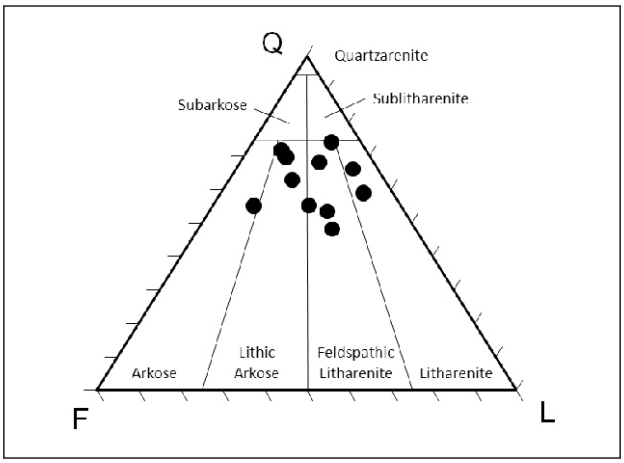

Figure 12. *Ternary diagram of sandstone petrographic composition (n=11). Sandstones of the Dycedale Syncline range from quartz-rich arkose to quartz-rich litharenite. Q=Quartz, F = Feldspar, L = Lithics including chert.*

Stratigraphic correlation

The distinctive marker unit of the Moodies Basaltic Lava (MdL2 of Anhaeusser, 1976) allows ready correlation of the stratigraphic column of the Dycedale Syncline with those of adjacent fault-bounded Moodies tectonic blocks (Figure 15), in particular to the Saddleback Syncline adjacent to the south, and to the Moodies Hills Block (and the Eureka Syncline contiguous with it) to the north. Correlations show significant differences, though: The thick, coarse-grained and very-large-scale cross-bedded quartzarenite unit MdQ2 (Visser et al., 1956; Anhaeusser, 1976) is not present in the Dycedale Syncline, whereas the thick alluvial conglomerate of Dycedale Syncline's Unit B has no equivalents in those two synclines.

It is surprising that such a small area should develop a distinct stratigraphy. This can perhaps best be explained by the syntectonic, fault-controlled nature of Moodies deposition in temporally restricted or isolated basins (Heubeck and Lowe, 1994a; Stutenbecker, 2014).

Sandstone provenance and diagenesis

Sandstone framework grains from the Dycedale Syncline, as other Moodies sandstones, are either intrabasinal, including Onverwacht and Fig Tree Group grain types, or extrabasinal, including monocrystalline plutonic quartz, plutonic feldspar and polycrystalline plutonic grains; in addition, volcanically derived sedimentary matrix is common (Heubeck and Lowe, 1999). In the sandstone composition ternary diagram of Folk (1965), Dycedale Syncline sandstones rich in chert and altered volcanics mostly plot in the lithic arkose and feldspathic litharenite field (Figure 12). The more matrix-rich sandstones grade into wackes.

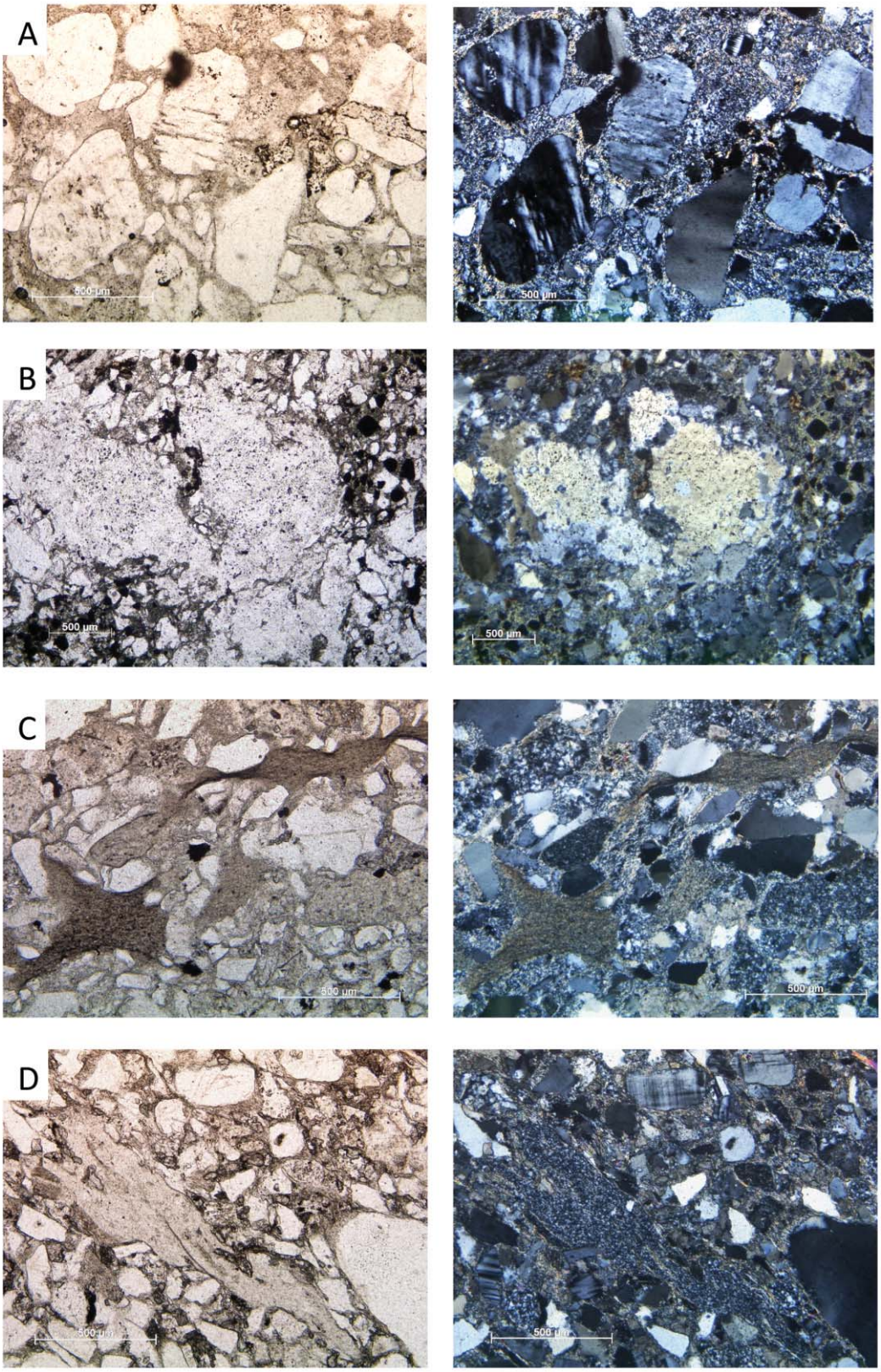

Figure 13. *Petrography of sandstone in the Dycedale Syncline. Left: Plane-polarized light; right: Cross-polarized light.* (***A***) *Matrix-rich arkose. (sample SB 04-14, unit H* (***B***) *Silicified gypsum nodules (light) in sandstone; opaque grains in heavy mineral lamination are largely pyrite. Microprobe data show that impurities in nodules are carbonate, barite and sulfate (Nabhan et al., 2016b). (sample SB 06-14, unit C)* (***C***) *Shale wisps in matrix-rich cherty sublitharenite indicating erosion of nearby shale and low degree of metamorphic overprint. (sample SB 09-14, unit F)* (***D***) *Large tuff clast (center left) composed of fine-grained sericite, chlorite and carbonate in matrix-rich lithic arkose. Note fresh microcline in top center. (sample SB 10-14, unit A)*

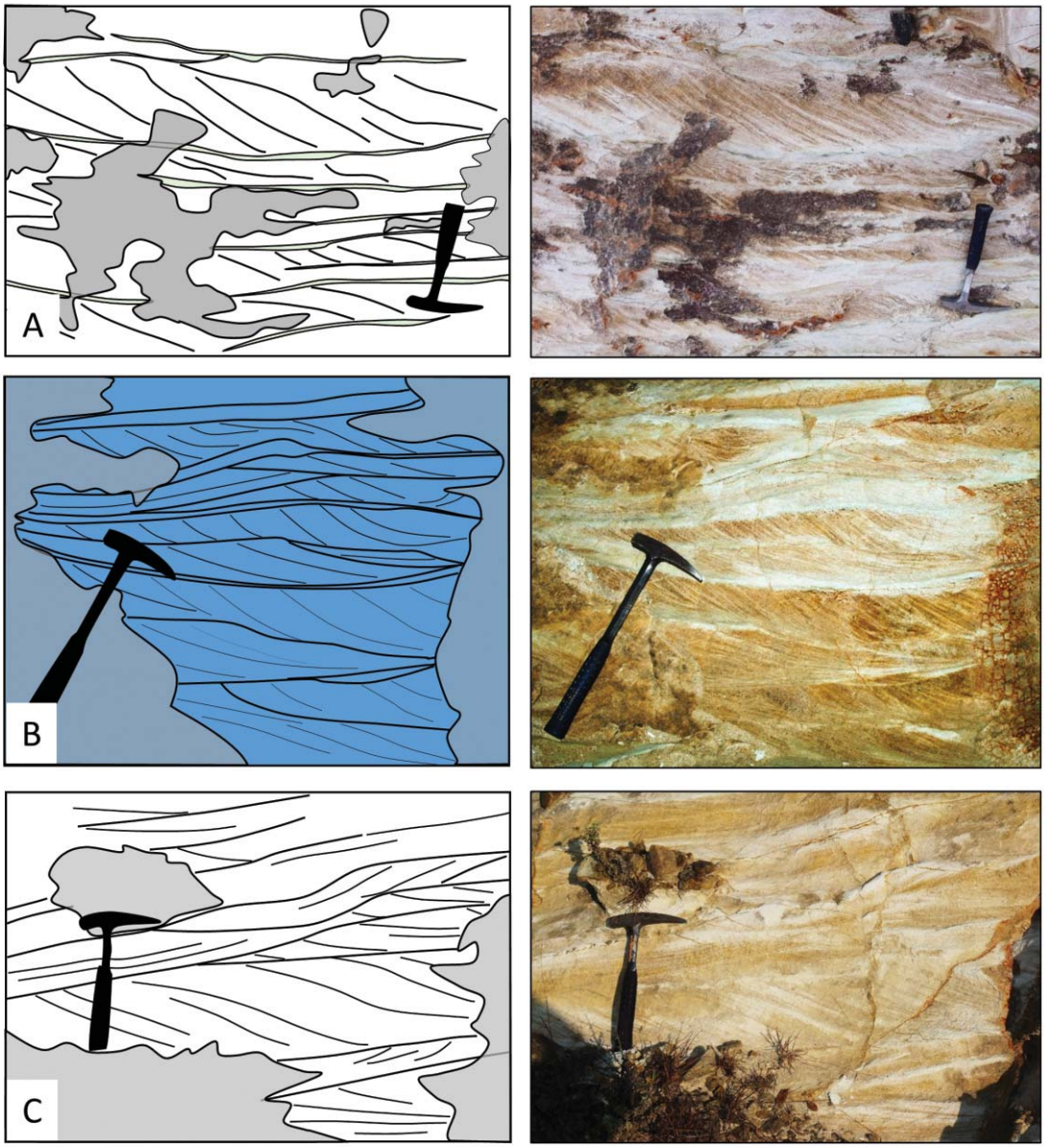

Figure 14. *Bedding architecture in sandstones of unit F (top), G (middle) and H (bottom). Outcrop photographs are shown to the right, line drawings to the left. Outcrops are nearly two-dimensional. (**A**) Unidirectional crossbedding interrupted by single mud coats, indicating a sedimentation in the fluvial-tidal transition zone (one slack period per tidal cycle). (**B**) Segments of complex, dominantly unidirectional dunes (sand waves), coated by thin mud coats. This pattern is characteristic of shallow subtidal settings. (**C**) Apparently bidirectional cross lamination lacking shale drapes. This may possibly be true herringbone bedding suggestive of a deep channel with strong but balanced ebb and flood flow.*

The high feldspar content of some sandstones is unusual, particularly so for Archean feldspathic sandstones that are generally assumed to have been subjected to rapid grain size reduction by intense chemical dissolution under an aggressive, CO_2-rich atmosphere (Hessler and Lowe, 2006; Sheldon, 2006). How can this unusual composition be explained? The rapid lateral facies changes and low textural maturity clearly indicate that Dycedale Syncline sandstones underwent little transport and reworking; they were quickly buried in a rapidly subsiding basin. Microbial mats, tuffs, and some shale all contributed to quickly reduce permeability and reduce feldspar dissolution even at a low depth of burial when pore waters became saturated with feldspar weathering products. Nabhan et al. (2016a) also argued that early silicification may have stiffened surficial strata early and prevented major compaction.

The muscovite-kaolinite composition of the tuffaceous matrix is likely a product of early diagenetic K-metasomatism of volcanic glass of dacitic composition, feldspar and poorly crystallized K-phyllosilicates at the sediment-water interface (Rouchon and Orberger, 2008; Rouchon et al., 2009), resulting in hydration, dissolution and neoformation of minerals. K-uptake would have been favored by low pH and a high temperature of seawater or hydrothermal fluids. Kaolinite, however, reacts to form dickite or pyrophyllite at <250°C. Its presence, despite indications of somewhat higher-grade greenschist-facies metamorphism nearby, can be explained by protection from

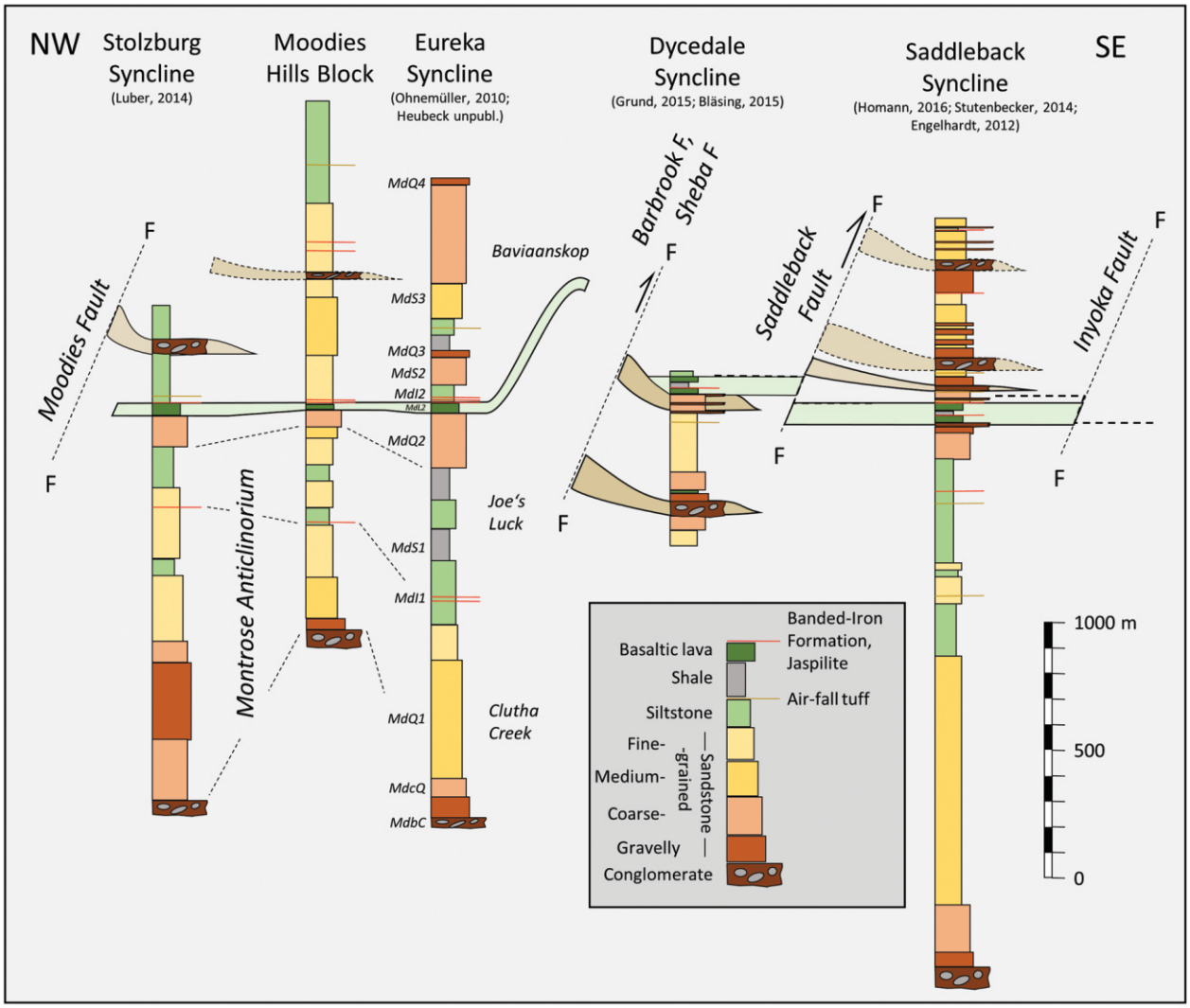

Figure 15. *Stratigraphic correlation diagram of Moodies Group lithologies between the major tectonic synclines in the BGB north of the Inyoka Fault.*

subsequent metamorphism by pervasive silicification, burial temperatures in the study area remaining below low anchizone conditions or recent weathering of feldspar and mica. There is no petrographic evidence for retrograde alteration of andalusite or pyrophyllite to kaolinite.

Volcanism

A complete review of volcanic contributions to the Moodies Group is beyond the scope of this manuscript. Despite the perception of the Moodies Group being a purely siliciclastic unit, diverse volcanic units and lithologies exist, although most of them are thin and/or discontinuous. Most Moodies volcanic units resemble Fig Tree volcanic rocks in type and composition. Within the BGB, they include about twenty individual, mappable but discontinuous rhyodacitic air-fall tuffs, at least one ignimbrite, and a regionally mappable mafic lava flow (Heubeck et al., 2013). Some Moodies sediments show a proximal volcanic provenance, evidenced by the common to abundant feldspar-porphyry clasts of Schoongezicht (uppermost Fig Tree Group) age in conglomerates, the tuffaceous admixture to sandstones, tuffaceous rip-up clasts, and the common to abundant QSM (quartz-sericite-mosaic) grains in sandstones. The Moodies Group contact to the underlying volcaniclastic and volcanic Schoongezicht Formation is gradational.

South of the Inyoka Fault, a large dyke network crosscut, deformed, and partially absorbed Moodies strata (Heubeck and Lowe, 1994b). Aside from these occurrences, however, Moodies strata have nowhere been shown to interfinger with or abut against volcanic strata. This is puzzling, but may in part be due to the overprinting of many facies contacts by faulting, and also due to the high degree of steepening, uplift and erosion. Overall, there is little doubt that Fig Tree-style volcanism continued into Moodies time but was overwhelmed by abundant extrabasinal siliciclastic contributions derived from quartz-rich granitoids. Dacitic and rhyodacitic volcanic activity in the lower Moodies Group is likely related to a deepening-upward extensional setting, while the Moodies basaltic lava, midway in the section, may indicate access to more mafic, hotter, and more deeply-seated melts.

Potassic and midly peraluminous magmatism may have accompanied BGB tectonics more than commonly thought

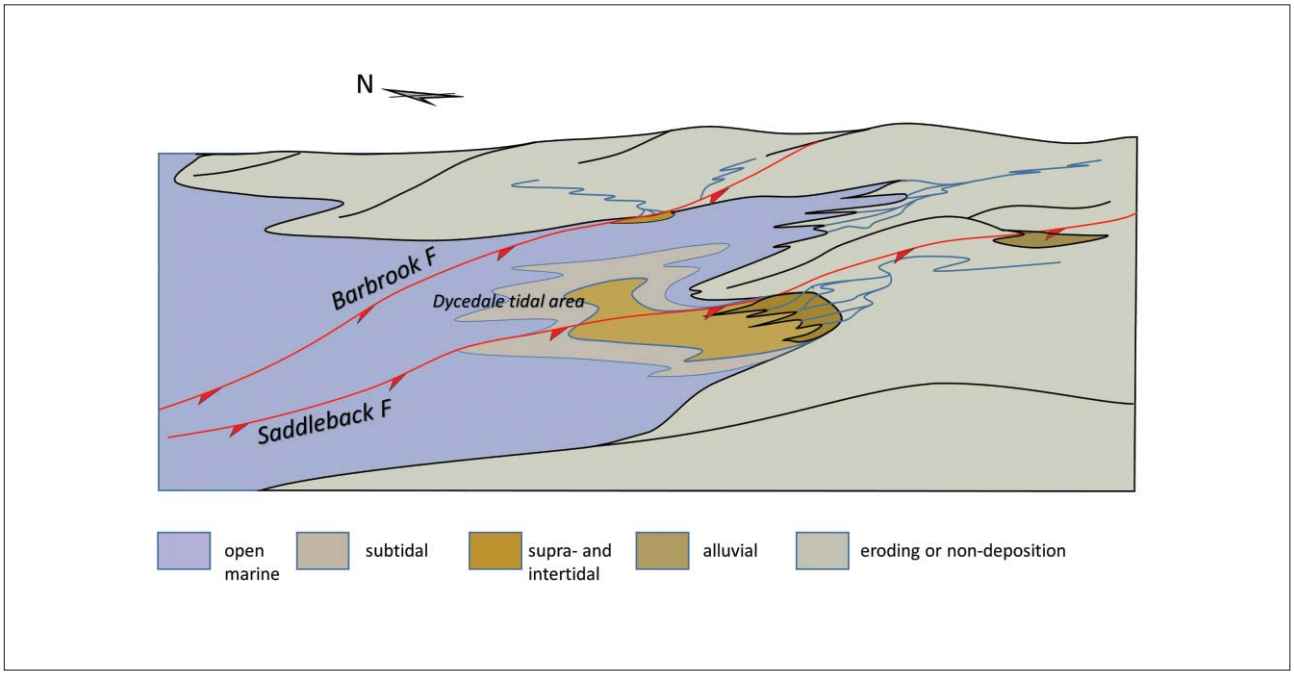

Figure 16. *Paleoenvironmental sketch of the Dycedale Syncline region. View towards the northeast.*

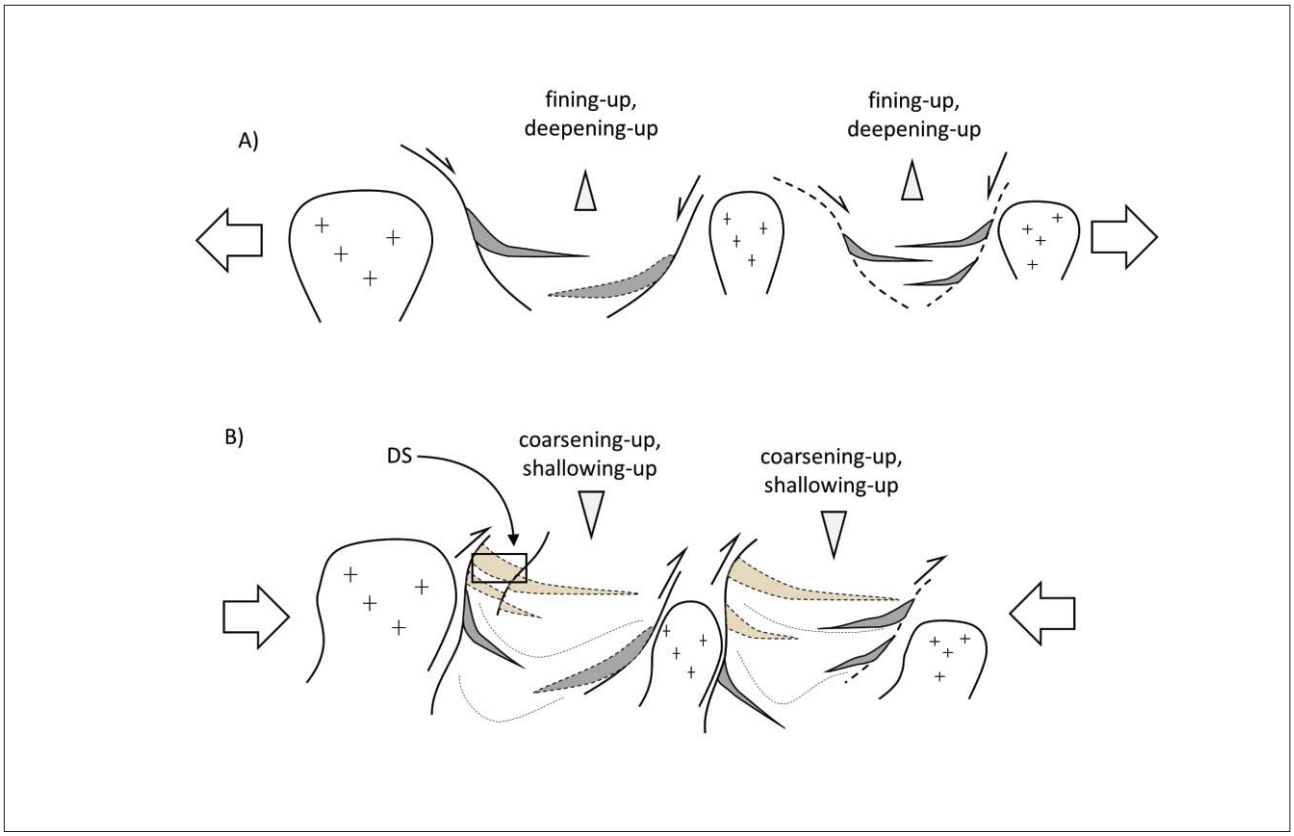

Figure 17. *Schematic north-south profiles showing two-phase evolution of Moodies Group strata in the BGB. DS = Dycedale Syncline. (**A**) Extensional phase: Moodies basins form in an overall extensional setting, marked by a fining- and deepening-upward trend, between rising plutons. (**B**) Shortening phase: Syndepositional reactivation of the same fault sets in a shortening sense leads to progressive unconformities along the basin margins and an overall shallowing- and coarsening-upward trend.*

(Sanchez-Garrido et al., 2011). These magmas left their records in rhyolites and dacites of the uppermost Hooggenoeg Formation (Onverwacht Group, ca. 3.445 Ga) and in the arkosic composition of middle Moodies Group sandstones which are ca. 3220 Ma old. Age-equivalent granites, however, have not been identified; Sanchez-Garrido et al. (2011) argue that these granitic Moodies source rocks were eroded due to their high-level crustal position.

Tectonic setting

The Dycedale Syncline is fault-bounded. The vertical offset between the Dycedale Syncline and the adjacent Saddleback Syncline to the south along the Saddleback Fault is minor. It can be readily estimated by the relative displacement of the Moodies Basaltic Lava to be approximately 150 m up-to-the-north. Displacement along the Barbrook Fault, the northern margin of the Dycedale Syncline, is also up-to-the-north but likely exceeds one km because Onverwacht and lower Fig Tree Group strata to the north are displaced against "middle" Moodies strata to the south. In a larger context, the Dycedale Syncline is thus essentially a tectonic sliver of the Saddleback Syncline, separated slightly from it by the Saddleback Fault, and with a distinctive stratigraphy (Figure 15).

The displacements could either have been created by north-to-south shortening (Heubeck and Lowe, 1994b), by overturning former down-to-the-south normal faults, or by a combination of both. Basin formation could initially have taken place in an extensional setting. The last major event, however, was clearly of a shortening type and folded Moodies strata into tight synclines separated by narrow, faulted anticlines. Evidence for basin-forming extension around 3225 Ma has been accumulating (Kisters et al., 2003, 2010; Lana et al., 2011), and Heubeck et al. (2013) argued that the final tightening and rotation of greenstone belt strata into the vertical was completed by 3219 ± 9 Ma, the age of an undeformed felsic dyke crosscutting vertical beds of uppermost Moodies siltstones in the Moodies Hills block west of Barberton.

A detailed assessment of the regional tectonic history cannot be derived from the Dycedale Syncline region alone, but requires a combination of regional synthesis and structural/geochronological analysis. Several lines of evidence, however, indicate the syndepositional deformation of the Dycedale Syncline, including the facies stacking in an apparently rapidly subsiding basin with limited stratigraphic continuity, alluvial fans interfingering with tidal zones, and the high feldspar content (Figures 16, 17).

Conclusions

The westernmost Dycedale Syncline showcases two important aspects of Archean geology: Its coherent stratigraphic column includes well-exposed and easily accessible strata representing a range of alluvial-to-subtidal environments, and its structural geology demonstrates the close interrelationship between sedimentation and tectonics at 3.2 Ga.

The siliciclastic and volcanic units include sections through a medium- to high-energy, arid coastal plain with shoreline and tide-dominated estuarine environments modified by ash-fall tuffs and lava flows. Microbial communities inhabited the subsurface vadose zone and surface environments where they coped with high current stresses, abrasion, air-fall tuffs, intensive UV-radiation and evaporation. The tidal range was moderate or higher but cannot be quantitatively constrained.

The Dycedale Syncline originally formed as a small basin in a subsequently steepened south-facing thrust belt that may have reactivated bounding faults of an earlier extensional system. Because the surface processes documented for the Archean environments in the Dycedale Syncline can – by and large – also be found regionally in less accessible and less well preserved regions of the BGB, it stands to reason that these processes may be more widely represented for considerable proportions of Archean surface environments in general.

Acknowledgments

We would like to thank Nico and Delia Oosthuizen for access to the Mountainlands Reserve and the Barberton Community for active interest and continued support. CH and MH were supported by DFG grant He2418/13-1, SN by DLR-Helmholtz Alliance "Planetary Evolution and Life" grant X/957/67147527 to CH. CH was also partially supported by the EU COST Action "Life-ORIGINS" (TD1308). MG and SB were supported by DAAD stipends. Constructive reviews by Axel Hofmann and an anonymous reviewer considerably improved the manuscript.

References

Allen, G.P., 1991. Sedimentary processes and facies in the Gironde estuary: a recent model for macrotidal estuarine systems. In: D.G. Smith, G.E. Reinson, B.A. Zatlin and R.A. Rahmani (Editors), Clastic Tidal Sedimentology. Canadian Society of Petroleum Geologists Memoir, 16, 29-40.

Allmendinger, R. W., Cardozo, N. C. and Fisher, D., 2013. Structural Geology Algorithms: Vectors and Tensors. Cambridge, England, Cambridge University Press, 289pp.

Anhaeusser, C. R., 1969. The stratigraphy, structure, and gold mineralization of the Jamestown and Sheba Hills areas of the Barberton Mountain Land. PhD thesis, University of the Witwatersrand, Johannesburg, 332pp.

Anhaeusser, C.R., 1976. The geology of the Sheba Hills area of the Barberton Mountain Land, South Africa, with particular reference to the Eureka Syncline. Transactions of the Geological Society of South Africa, 79, 253-280.

Archer, A., 1996. Reliability of lunar orbital periods extracted from ancient cyclic tidal rhythmites. Earth and Planetary Science Letters, 141, 1-10.

Archer, A., 2013. World's highest tides: Hypertidal coastal systems in North America, South America and Europe. Sedimentary Geology, 284-285, 1-25.

Ashwal, L.D. (Editor), 1991. Two Cratons and an Orogen - Excursion Guidebooks and Review Articles for a Field Workshop through Selected Archaean Terranes of Swaziland, South Africa and Zimbabwe. IGCP Project 280, Department of Geology, University of the Witwatersrand, Johannesburg, 312pp.

Bläsing, S., 2015. Petrography and sedimentology of selected sandstones of the westernmost Dycedale Syncline, Barberton Greenstone Belt, South Africa. B.Sc thesis, Freie Universität Berlin, 38pp.

Bläsing, S., Grund, M. and Heubeck, C., 2015. Petrography and structural geology of the westernmost Dycedale Syncline (Barberton Greenstone Belt, South Africa) – Implications for Archean tectonics and depositional environments. DGGV / DMG Annual Meeting, Berlin, Abstract Volume, 86.

Bucher, K. and Frey, M., 1994. Petrogenesis of metamorphic rocks. Springer (New York Heidelberg), 318p.

Coughenour, C.L., Archer, A.W. and Lacovara, K.J., 2009. Tides, tidalites, and secular changes in the Earth–Moon system. Earth-Science Reviews, 97, 59-79.

Dalrymple, R.W. and Rhodes, R.N., 1995. Estuarine dunes and bars. In: G.M.E. Perillo (Editor). Geomorphology and sedimentology of estuaries. Elsevier, Amsterdam, 359-422.

Dalrymple, R.W. and Choi, K., 2007. Morphologic and facies trends through the fluvial-marine transition in tide-dominated depositional systems. A schematic framework for environmental and sequence-stratigraphic interpretation. Earth-Science Reviews, 81, 135-174.

De Ronde, C.E.J. and de Wit, M.J., 1994. Tectonic history of the Barberton Greenstone Belt, South Africa: 490 million years of Archaean evolution. Tectonics, 13, 983-1005.

Dickinson, W.R. and Suczek, C.A., 1979. Plate Tectonics and Sandstone Compositions. American Association of Petroleum Geologists Bulletin, 63, 2164-2182.

Dickinson, W.R., Beard, L.S., Brakenridge, G.R., Erjavec, J.L., Ferguson, R.C., Inman, K.F., Knepp, R.A., Lindberg, F.A. and Ryberg, P.T., 1983. Provenance of North American Phanerozoic sandstones in relation to tectonic setting. Geological Society of America Bulletin, 94, 222-235.

Eisma, D., 1997. Intertidal Deposits: River mouths, tidal flats, and coastal lagoons. CRC Marine Science Series, CRC Press (Boca Raton, Boston, London, New York, Washington DC), 525pp.

Engelhardt, J.F., 2012. Constraints from high-resolution zircon geochronology on age and provenance of the Archean Moodies Group, Barberton Greenstone Belt, South Africa. M.Sc. thesis, Freie Universität Berlin, 88pp.

Eriksson, K.A., 1977. Tidal deposits from the Archean Moodies Group, Barberton Mountain Land, South Africa. Sedimentary Geology, 18, 257-281.

Eriksson, K.A., 1978. Alluvial and destructive beach facies from the Archaean Moodies Group, Barberton Mountain Land, South Africa and Swaziland. In: A.D. Miall (Editor), Fluvial Sedimentology. Canadian Society of Petroleum Geologists, Memoir, 5, 287-311.

Eriksson, K.A., 1979. Marginal marine depositional processes from the Archaean Moodies Group, Barberton Mountain Land, South Africa: Evidence and significance. Precambrian Research, 8, 153-182.

Eriksson, K., 1980. Transitional sedimentation styles in the Moodies and Fig Tree Groups, Barberton Mountain Land, South Africa: evidence favouring an Archean continental margin. Precambrian Research, 12, 141-160.

Eriksson, K.A. and Simpson, E.L., 2002. Quantifying the oldest tidal record: The 3.2 Ga Moodies Group, Barberton Greenstone Belt, South Africa. Geology, 28, 831-834.

Eriksson, K. A., Simpson, E. L. and Mueller, W., 2006. An unusual fluvial to tidal transition in the mesoarchean Moodies Group, South Africa: A response to high tidal range and active tectonics. Sedimentary Geology, 190, 13-24.

Eriksson, P.G., Bumby, A.J. and Popa, M., 2004. Sedimentation through time; In: P.G. Eriksson, W. Altermann, D.R. Nelson, W.U. Mueller and O. Catuneanu, (Editors). The Precambrian Earth: Tempos and Events. Developments in Precambrian Geology, 12 (Elsevier), 593-612.

Ferrar, T. and Heubeck, C., 2013. Barberton-Makhonjwa Geotrail; Geosites and view points. Hamilton-Fynch for Batobic, Mbombela/Nelspruit, South Africa, 44p.

Fenies, H., De Resseguier, A. and Tastet, J.P., 1999. Intertidal clay-drape couplets (Gironde estuary, France). Sedimentology, 46, 1-15.

Folk, R.L., 1965. Petrology of Sedimentary Rocks., Hemphill, Austin, Texas.

Gay, N.C., 1969. The analysis of strain in the Barberton Mountain Land, eastern Transvaal, using deformed pebbles. Journal of Geology (London), 77, 377-396.

Grund, M., 2015. Stratigraphy and Structural Geology of the Westernmost Dycedale Syncline (Moodies Group, Barberton Greenstone Belt, South Africa). B.Sc.-thesis, Freie Universität Berlin, 33pp.

Habicht, K. and Canfield, D., 1996. Sulphur isotope fractionation in modern microbial mats and the evolution of the sulphur cycle. Nature, 382, 342-343.

Hall, A.L., 1918. The Geology of the Barberton Gold Mining District. Geological Survey of South Africa Memoir, 9, 347pp.

Hessler, A.M. and Lowe, D.R., 2006. Weathering and sediment generation in the Archaean: An integrated study of the evolution of siliciclastic sedimentary rocks of the 3.2 Ga Moodies Group, Barberton Greenstone Belt, South Africa. Precambrian Research, 151, 185-210.

Heubeck, C., 2009. An early ecosystem of Archean tidal microbial mats (Moodies Group, South Africa, ca. 3.2 Ga). Geology, 37, 931-934.

Heubeck, C. and Lowe, D.R., 1994a. Depositional and tectonic setting of the Archean Moodies Group, Barberton Greenstone Belt, South Africa. Precambrian Research, 68, 257-290.

Heubeck, C. and Lowe, D.R., 1994b. Late syndepositional deformation and detachment tectonics in the Barberton Greenstone Belt, South Africa. Tectonics, 13, 1514-1536.

Heubeck, C. and Lowe, D.R., 1999. Sedimentary petrography and provenance of the Archean Moodies Group, Barberton Greenstone Belt. In: D.R. Lowe, and G.R. Byerly (Editors). Geologic Evolution of the Barberton Greenstone Belt, South Africa. Geological Society of America Special Paper, 329, 259-286.

Heubeck, C., Engelhardt, J., Byerly, G.R., Zeh, A., Sell, B., Luber, T. and Lowe, D.R., 2013. Timing of deposition and deformation of the Moodies Group (Barberton Greenstone Belt, South Africa): Very-high-resolution of Archaean surface processes. Precambrian Research, 231, 236-262.

Heubeck, C., Köhler, I., Homann, M. and Drabon, N., 2015. Raman Spectroscopy of biomats from the Moodies Group (Barberton Greenstone Belt, South Africa, 3.22 Ga). Conference abstract, Habitability in the Universe: From the Early Earth to Exoplanets, 22-27 March 2015, Porto, Portugal, 66.

Homann, M., 2016. Depositional setting and metabolism of microbial mats in the Archean Moodies Group, Barberton Greenstone Belt, South Africa. PhD thesis, Freie Universität Berlin, 105pp.

Homann, M., Heubeck, C., Airo, A. and Tice, M.M., 2015. Morphological adaptations of 3.22 Ga-old microbial communities to Archean coastal habitats (Moodies Group, Barberton Greenstone Belt, South Africa). Precambrian Research, 266, 47-64.

Kappler, A, Pasquero, C., Konhauser, K.O. and Newman, D.K., 2005. Deposition of banded iron formations by anoxygenic phototrophic Fe(II)-oxidizing bacteria. Geology, 33, 865-868.

Kisters, A.F.M., Stevens, G., Dziggel, A. and Armstrong, R.A., 2003. Extensional detachment faulting and core complex formation in the southern Barberton granite-greenstone terrain, South Africa: evidence for a 3.2 Ga orogenic collapse. Precambrian Research, 127, 355-78.

Kisters, A.F.M., Belcher, R.W., Poujol, M. and Dziggel, A., 2010. Continental growth and convergence-related arc plutonism in the Mesoarchaean: Evidence from the Barberton granitoid-greenstone terrain, South Africa. Precambrian Research, 178, 15-26.

Lamb, S., 1987. Archean synsedimentary tectonic deformation – A comparison with the Quaternary. Geology, 15, 565-568.

Lana, C., Buick, I., Stevens, G., Roussow, R. and de Wet, W., 2011. 3230-3200 Ma post-orogenic extension and mid-crustal magmatism along the southeastern margin of the Barberton Greenstone Belt, South Africa. Journal of Structural Geology, 33, 844-858.

Leclair, S.F. and Bridge, J.S., 2001. Quantitative Interpretation of Sedimentary Structures Formed by River Dunes. Journal of Sedimentary Research, 71, 713-716.

Lowe, D.R. and Byerly, G.R., 2003. Field guide to the geology of the 3.5-3.2 Ga Barberton Greenstone Belt, South Africa: A guidebook prepared for a field conference. Archean Surface Processes, June 23-July 2, 2003, 184pp.

Lowe, D.R. and Byerly, G.R., 2007. An overview of the geology of the Barberton Greenstone Belt and vicinity: Implications for early crustal development. In: M.J. Van Kranendonk, R.H. Smithies and V. Bennett (Editors). Earth's Oldest Rocks, Developments in Precambrian Geology, 15, Elsevier, Amsterdam, 481–526.

Lowe, D.R. and Nocita, B.W., 1999. Foreland basin sedimentation in the Mapepe Formation, southern-facies Fig Tree Group. In: D.R. Lowe and G.R. Byerly (Editors). Geologic Evolution of the Barberton Greenstone Belt. Geological Society of America Special Paper, 329, 233-258.

Lowe, D.R., Byerly, G.R. and Heubeck, C., 2012. Geologic Map of the west-central Barberton Greenstone Belt, South Africa, scale 1:25,000. Geological Society of America Map and Chart Series, No. 103.

Luber, T., 2014. Archaean Geology of the east-central Stolzburg Syncline, Barberton Greenstone Belt, South Africa. M.Sc.-thesis, Freie Universität Berlin, 78pp.

Martinius, A.W. and van den Berg, J.H., 2011. Atlas of sedimentary structures in estuarine and tidally-influenced river deposits of the Rhine-Meuse-Scheldt system: Their application to the interpretation of analogous outcrop and subsurface depositional systems. European Association of Geophysicists and Engineers (EAGE) Publications, Houten, The Netherlands, 298pp.

Mazumder, R. and Arima, M., 2005. Tidal rhythmites and their implications. Earth-Science Reviews, 69, 79-95.

Nabhan, S., Luber, T., Scheffler, F. and Heubeck, C., 2016a. Climatic and geochemical implications of Archean pedogenic gypsum in the Moodies Group (~3.2 Ga), Barberton Greenstone Belt, South Africa. Precambrian Research, 275, 119-134.

Nabhan, S., Wiedenbeck, M., Milke, R. and Heubeck, C., 2016b. Biogenic overgrowth on detrital pyrite in 3.2 Ga Archean paleosols. Geology, 44, 763-766..

Nio, S.D. and Yang, C.S., 1991. Diagnostic attributes of clastic tidal deposits: a review. In: D.G. Smith, G.E. Reinson, B.A. Zaitlin and R.A. Rahmani (Editors). Clastic Tidal Sedimentology. Canadian Society of Petroleum Geologists Memoir, 16, 3-28.

Noffke, N., Eriksson, K.A., Hazen, R.M. and Simpson, E.L., 2006. A new window into Early Archaean life: Microbial mats in Earth's oldest siliciclastic tidal deposits (3.2 Ga Moodies Group, South Africa). Geology, 34, 253-256.

Ohnemueller, F., 2010. Implications of below-wavebase sedimentation in the Moodies Group, Barberton Greenstone Belt, South Africa. M.Sc.-thesis, Freie Universität Berlin, 74pp.

Olsson, J. R., Soderlund, U., Klausen, M. B. and Ernst, R.E., 2010. U-Pb baddeleyite ages linking major Archean dyke swarms to volcanic-rift forming events in the Kaapvaal craton (South Africa), and a precise age for the Bushveld Complex. Precambrian Research, 183, 490-500.

Pearton, T.N., 1986 (Compiler, Editor). Geocongress '86 – Excursion Guidebook for Barberton Mountain Land - Excursion 17 - and Barberton Gold - Excursion 18. Geological Society of South Africa, ISBN 0-620-09807-4, 83pp.

Sanchez-Garrido, C., Stevens, G., Armstrong, R.A., Moyen, J.-F., Martin, H. and Doucelance, R., 2011. Diversity in Earth's early felsic crust: Paleoarchean peraluminous granites of the Barberton Greenstone Belt. Geology, 39, 963-966.

Sheldon, N.D., 2006. Precambrian paleosols and atmospheric CO_2 levels. Precambrian Research, 147, 148-155.

Stutenbecker, L., 2014. Sedimentology, petrography and provenance of the 'Lomati Quartzite': Implications for syntectonic Moodies Group sedimentation, Barberton Greenstone Belt, South Africa. MSc. Thesis, Freie Universität Berlin, 70pp.

Tice, M.M., Bostick, B.C. and Lowe, D.R., 2004. Thermal history of the 3.5-3.2 Ga Onverwacht and Fig Tree Groups, Barberton greenstone belt, South Africa, inferred by Raman microspectroscopy of carbonaceous material. Geology, 32, 37-40.

Toulkeridis, T., Goldstein, S.L., Clauer, N., Kröner, A., Todt, W. and Schidlowski, M. 1998. Sm–Nd, Rb–Sr and Pb–Pb dating of silicic carbonates from the early Archaean Barberton Greenstone Belt, South Africa: Evidence for post-depositional isotopic resetting at low temperature. Precambrian Research, 92, 129-144.

Van den Berg, J.H., Boersma, J.R. and van Gelder, A., 2007. Diagnostic sedimentary structures of the fluvial–tidal transition zone. Evidence from deposits of the Rhine Delta. Netherlands Journal of Geosciences - Geologie en Mijnbouw, 86, 287-306.

Visser, D.J.L. (compiler), 1956. The Geology of the Barberton area. Special Publication of the Geological Society of South Africa, 15, 253pp.

Ward, J.H.W., 1995. Geology and Metallogeny of the Barberton Greenstone Belt - a Survey. Journal of African Earth Sciences, 21, 213-240.

Williams, G.E., 2000. Geological constraints on the Precambrian history of Earth's rotation and the Moon's orbit. Reviews of Geophysics, 38, 37-59.

Editorial handling: L.D. Ashwal